DOT/FAA/TC-23/24

Federal Aviation Administration
William J. Hughes Technical Center
Aviation Research Division
Atlantic City International Airport
New Jersey 08405

Assessment of Emerging Metallic Structures Technologies through Test and Analysis of Fuselage Structure: Panel 2

July 2023

Final report

NOTICE

This document is disseminated under the sponsorship of the U.S. Department of Transportation in the interest of information exchange. The U.S. Government assumes no liability for the contents or use thereof. The U.S. Government does not endorse products or manufacturers. Trade or manufacturers' names appear herein solely because they are considered essential to the objective of this report. The findings and conclusions in this report are those of the author(s) and do not necessarily represent the views of the funding agency. This document does not constitute FAA policy. Consult the FAA sponsoring organization listed on the Technical Documentation page as to its use.

This report is available at the Federal Aviation Administration William J. Hughes Technical Center's Full-Text Technical Reports page: actlibrary.tc.faa.gov in Adobe Acrobat portable document format (PDF).

Form DOT F 1700.7 (8-72) Reproduction of completed page authorized

1. Report No.	2. Government Accession No.	3. Recipient's Catalog No.
DOT/FAA/TC-23/24		

4. Title and Subtitle	5. Report Date
Assessment of Emerging Metallic Structures Technologies through Test and Analysis of Fuselage Structure: Test Panel 2	July 2023
	6. Performing Organization Code: ANG-E281
7. Author(s): Yongzhe Tian, Dave Stanley, John Bakuckas Jr., Mike Kulak, Erin Fulton	8. Performing Organization Report No.
9. Performing Organization Name and Address: William J. Hughes Technical Center, Federal Aviation Administration, Aviation Research Division, Structures and Materials Section, Atlantic City International Airport, NJ 08405	10. Work Unit No. (TRAIS)
	11. Contract or Grant No.
12. Sponsoring Agency Name and Address: U.S. Department of Transportation, Federal Aviation Administration, FAA Transport Airplane Directorate, Airframe/Cabin Safety, ANM-115, 1601 Lind Avenue SW, Renton, WA 98057	13. Type of Report and Period Covered: Final Report
	14. Sponsoring Agency Code

15Supplementary Notes

16. Abstract

In partnership with Arconic and Embraer, the Federal Aviation Administration (FAA) is assessing emerging metallic structures technologies (EMST) using the FAA's Full-Scale Aircraft Structural Test Evaluation and Research (FASTER) facility and Structures and Materials Lab Full-scale fuselage panel test data will be obtained to assess the effect of EMST fuselage concepts on damage tolerance performance as compared to the baseline aluminum fuselage structures located on the crown of a typical single-aisle aircraft forward of the wing. Several technologies will be considered in the scope of the project, including advanced aluminum–lithium alloys and selective reinforcement using fiber metal laminates. Data from this study will be used to verify improved weight and structural safety performance of EMST and to assess the adequacy of existing airworthiness standards and guidance needed for the implementation of arising technologies and their impact on future designs. Results from the second panel test are summarized and compared with the baseline panel 1 in this technical note and will be compared to future tests on advanced panels containing varying EMST to assess the damage-tolerance performance.

17. Key Words	18. Distribution Statement
FASTER, Advanced Technologies, Damage Tolerance, Residual Strength, Finite Element Modeling, Aircraft Fuselage Structure	This document is available to the U.S. public through the National Technical Information Service (NTIS), Springfield, Virginia 22161. This document is also available from the Federal Aviation Administration William J. Hughes Technical Center at actlibrary.tc.faa.gov.

19. Security Classif. (of this report)	20. Security Classif. (of this page)	21. No. of Pages	22. Price
Unclassified	Unclassified	66	

Contents

Figures

Tables

Acronyms

Acronym	Definition
DIC	Digital Image Correlation
EMST	Emerging Metallic Structures Technologies
FAA	Federal Aviation Administration
FASTER	Full-Scale Aircraft Structure Test Evaluation and Research
FCG	Fatigue Crack Growth
FEA	Finite Element Analysis
FEM	Finite Element Modeling
SHM	Structural Health Monitoring
SRM	Structural Repair Manual

Executive summary

In partnership with Arconic and Embraer, the Federal Aviation Administration (FAA) is assessing emerging metallic structures technologies (EMST) using the FAA's Full-Scale Aircraft Structural Test Evaluation and Research (FASTER) facility and Structures and Materials Lab. Full-scale fuselage panel test data will be obtained to assess the effect of EMST fuselage concepts on damage tolerance performance, as compared to the current baseline aluminum fuselage structures, located on the crown of a typical single-aisle aircraft, forward of the wing. Several technologies were considered in the scope of the project, including advanced aluminum-lithium alloys and selective reinforcement using fiber metal laminates. Data from this study will be used to verify improved weight and structural safety performance of EMST and provide guidance needed for the implementation of arising technologies and their impact on future designs.

Results from panel 2 test are summarized in this technical note. A phased approach was undertaken for panel 2 to study two scenarios simulating damage that represents cracks in the structure: (1) a two-bay crack-like notch in the skin along the circumferential direction, with central stringer severed; (2) a two-bay crack-like notch in the longitudinal direction, with the central frame severed.

The results will be compared to the baseline panel 1 and future tests on advanced panels containing varying EMST to assess the damage-tolerance performance.

1 Introduction

The aircraft industry is striving to both improve performance and reduce costs in fabrication, operations, and maintenance by introducing advanced materials in conjunction with innovative manufacturing and production technologies. In light of the structural material decision made for the B787 and A350 airframe, and increasing competition from composite materials, the aluminum industry has made significant advancements over the past decade in developing new lightweight alloys and product forms, improved structural concepts, and manufacturing processes aimed at being competitive with composite materials in terms of manufacturing cost and performance. Collectively, these advances fall under the umbrella classification of emerging metallic structures technologies (EMST). Substantial investments have been made to demonstrate the potential to design and build durable and damage-tolerant fuselage and wing structures using EMST, including advanced alloys (Prasad, Gokhale, & Wanhill, 2014; Stonaker, Bakucka, & Freisthler, 2015), bonding and joining methods (Bertoni, Fernandez, & Miyazaki, 2014; Chaves, 2017; Kok, Poston, & Moore, 2011; Schmidt, 2005), and metallic-composite hybrids (Bertoni, Fernandez, & Miyazaki, 2014; Beumler, 2014; Chaves, 2017; Heinimann, et al., 2007; Schmidt, 2005; Silva, et al., 2017).

However, the introduction of a new material or concept in the aerospace industry can be quite challenging. A significant amount of test data at the coupon, substructure, and full-scale level is needed to fully vet and properly assess a new technology and understand potential certification and continued airworthiness issues. This includes the assessment of existing regulations and guidance materials to determine if the FAA needs to revise them or create new safety standards or guidance materials. For these reasons, regulators and industry ideally should work together in preparation for the application and certification of EMST.

In recognizing these challenges, the Federal Aviation Administration (FAA), Arconic, and Embraer are collaborating in a research effort to evaluate EMST for fuselage applications through full-scale testing and analysis. The goal is to assess and verify that the EMST have improved durability and damage tolerance compared with the current baseline aluminum fuselage located on the crown of a typical single-aisle aircraft forward of the wing spar. Several EMST are being considered, including integral frames, new metallic alloys, and selective reinforcement using fiber metal laminates. Fuselage panels with various EMST will be designed, fabricated, and tested in this multi-year effort, as shown in Figure 1. Panels will be tested using the FAAs Full-Scale Aircraft Structural Test Evaluation and Research (FASTER) facility, which was designed for testing fuselage panels and is capable of simulating aircraft service load

conditions through synchronous application of mechanical and environmental load conditions (Tian & Backuckas, 2019), Figure 2.

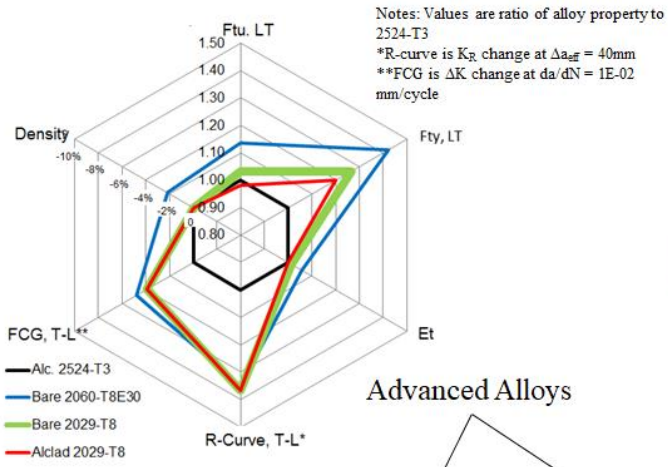

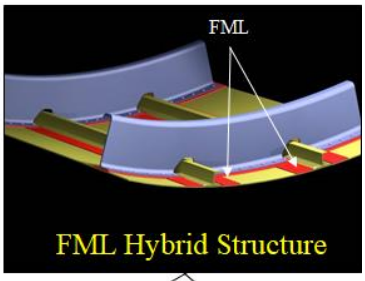

Advanced Alloys

		1 Baseline	2 Advanced Density Reduction	3 Advanced Materials	4 FML Reinforced	5 FML Reinforced (Optimized for Weight)
Component	Skin	2524-T3 sheet	2060-T8E30 Al-Li sheet	2029-T3 sheet	2524-T3 sheet	2524-T3 sheet
	Stringer	7150-T77511 extrusions, riveted	2055-T84 Al-Li extrusions, riveted	2055-T84 Al-Li extrusions, riveted	7150-T77511 extrusions, with FML straps	7150-T77511 extrusions, with FML straps
	Frame	7075-T62 - shear tied, extruded, riveted	2099-T83 Al-Li integral extrusions, riveted	2099-T83 Al-Li integral extrusions, riveted	7075-T62 - shear tied, extruded with FML straps	7075-T62 - shear tied, extruded with FML straps
Schedule	Start	Oct-17	Jan - 19	June - 21	Sep - 23	Jan - 25
	Finish	Dec-18	May -21	Aug - 23	Dec – 24	Dec - 25

Figure 1. Potential EMST test matrix

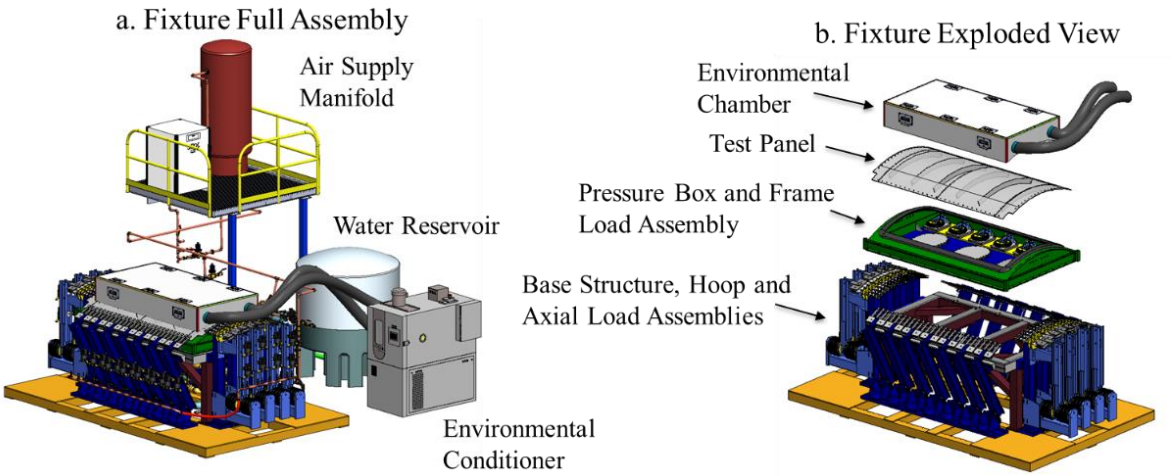

Figure 2. FAA FASTER fixture assembly and major component

A phased approach will be undertaken to study several damage scenarios, including: (1) a two-bay skin notch, along the circumferential direction, with central stringer severed; and (2) a two-bay skin notch, along the longitudinal direction, with the central frame severed. For each damage scenario phase, strain surveys will first be conducted and compared to finite element predictions to verify proper load and panel alignment. The panels will then be subjected to fatigue crack growth (FCG) testing using an equivalent constant-amplitude load sequence determined through coupon-level tests that represent the complex load history of a fuselage panel located on the crown of the aircraft, forward of the wing (Kulak, et al., 2024; Stonaker, et al., 2019). To demonstrate potential improvements in operational usage when considering aircraft equipped with EMST, an elevated fuselage pressure differential was used in the load sequence, which is approximately 15% higher than that used in a typical single-aisle transport category aircraft, such as the B737 and A320. The final stage of testing will be a residual strength test to limit load conditions identified in 14 CFR 25.571 (Damage-tolerance... , 2023). Data from this program will be used to demonstrate the improvement in damage tolerance and structural safety potential of EMST and provide guidance when considering EMST use.

This report documents results from tests conducted on the second panel, consisting of 2060-T80 skin, 2055-T84 stringers, and 2099-T83 integral frames. Panel 2 was subjected to two phases of testing and accumulated 85,920 simulated flights over an 18-month period. The phase 1 fatigue test has been paused for 5 months due to COVID-19 lockdown. Crack growth was monitored and recorded during all phases of testing using high-magnification cameras, several nondestructive inspection methods, strain gages, and a digital image correlation (DIC) system. For each phase, prior damage was repaired. Results from panel 2 tests are summarized below and will be compared with baseline panel 1 (Tian, Stanley, & Backuckas, 2021) and advanced panels containing varying EMST to assess the damage tolerance performance:

- **Phase 1**: A two-bay crack-like notch in the circumferential direction having a total length (tip-to-tip) of 1.3 in. was machined in the skin with the central stringer severed. The panel was then fatigue tested under simulated flight load conditions for 48,850 cycles in which slow and stable crack growth occurred to a final total length of 11.3 in. During the subsequent test conducted up to approximately 2.5 g (g-force) axial limit load, local stable tearing extension occurred from each crack-tip.
- **Phase 2**: A two-bay crack-like notch in the longitudinal direction having a total length of 3.25 in. was machined in the skin with the central frame severed and then fatigue tested to 37,070 cycles. During the fatigue test, the crack extended across two frame bays to a final length of 15.6 in. Afterwards, a residual strength test was conducted during which the panel failed at an applied pressure of 14 psi.

2 Experimental procedure

Testing for this program was conducted using the FAA's FASTER facility. A description of the test panel, test phases, applied loads, inspection, and monitoring methods are outlined in this chapter.

2.1 Target application and panel description

The target aircraft considered in this study is a typical single-aisle airplane, such as the B737 or A320. The location of the fuselage panel is assumed to be the crown just forward of the wing, where the major modes of loading are pressurization and vertical bending due to flight and landing loads. LMI Aerospace was contracted by Arconic to fabricate the baseline panel using standard aerospace manufacturing practices, including but not limited to forming, chemical milling, surface treatment, and joining technologies. The test article, panel 2, was fabricated per drawings provided in Appendix A.

The final panel dimensions were 125 in. × 76 in. with a radius of 74 in., as shown in Figure 3. The skin material was 2060-T8 with a pocketed construction, where the skin thickness was 0.050 in. in the mid-bay regions and 0.065 in. in the pad-up regions under the frames and stringers. Note that the panel was designed to have pocket skin thickness of 0.055 in. with a build tolerance of 0.005 in. and was discovered later to have an average of 0.050 in. The impact of thickness difference is addressed by (Kulak, et al., 2024). The substructure included eight stringers made from 2055-T84 extruded in a Z-section with a 7 in. spacing and six 2099-T8 integral frames connected using 2099-T8 shear ties with a 20 in. spacing. Reinforcing doublers were installed along the outer perimeter of the skin and to the frame ends for load attachment

points of the fixture. Holes of 0.5 in. diameter were drilled along the reinforced doubler edge of the panel for load introductions in the axial and hoop directions. Loads were also introduced into each frame. The major panel dimensions are listed in Table 1. The materials used for the major components are listed in Table 2.

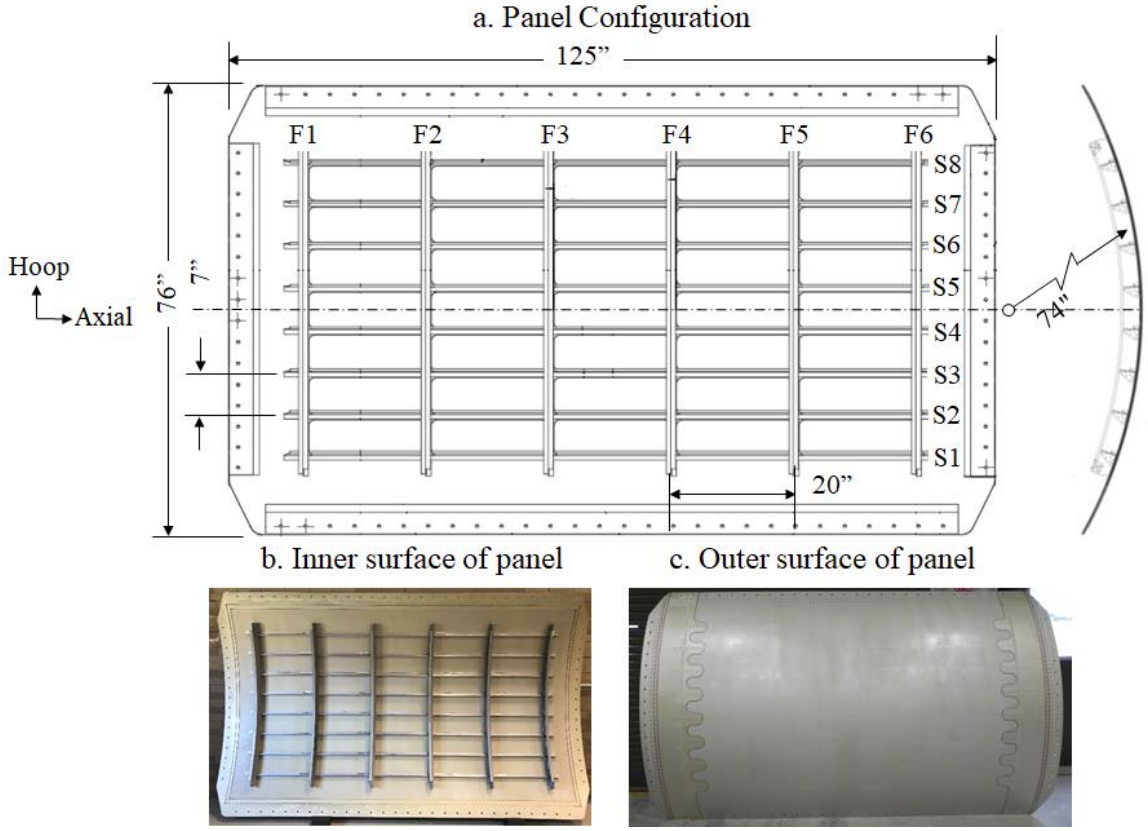

Figure 3. Panel 2 configuration and views of the internal and external surface

Table 1. Panel 2 dimensions

Panel length	125 in.
Panel width	76 in.
Panel radius	74 in.
Panel skin thickness, pad-up	0.065 in.
Panel skin thickness, mid-bay	0.050 in.
Number of frames	6
Number of stringers	8
Frame spacing	20 in.
Stringer spacing	7.0 in.

Table 2. Component materials used to fabricate panel 2

Component	Material
Skin	2060-T8 sheet
Stringer	2055-T84 extrusions, riveted
Frame	2099-T83 extrusions, riveted

2.2 Test phases and damage scenarios

A phased approach was undertaken to study the two damage scenarios summarized as follows.

Phase 1: Initial damage consisted of a crack-like notch having a length of 1.3 in. in the circumferential direction spanning two skin bays between frames F2 and F3, with the central stringer S4 severed (see Figure 4 Phase 1). Strain surveys were conducted to ensure proper load introduction. The panel was then fatigue tested under loads representing pressure, flight maneuver and gust accelerations, and landing loads in the forward crown section of a single-aisle aircraft. Fatigue testing was conducted until the crack extended to a final total length of 11.3 in. Afterwards, a limit load test was conducted, during which the panel was subjected to approximately 2.5 g axial load while holding the pressure constant under operational conditions. The panel was then repaired for follow-on phases (Appendix B).

Phase 2: Initial damage consisted of a two-bay longitudinal crack-like notch between stringers S6 and S7, with the central frame/shear tie F4 severed, as shown in Figure 4**,** Phase 2. A 3.25 in. long notch was inserted with the underneath frame severed. Initial strain surveys and finite element analysis (FEA) were conducted to ensure proper load introduction and to verify no effects from the repairs made in Phases 1. The panel was then fatigue tested, simulating pressure-only operational conditions, until the crack extended to a final length of approximately 16 in. A residual strength test was finally conducted to failure, measuring the load-carrying capacity of the panel.

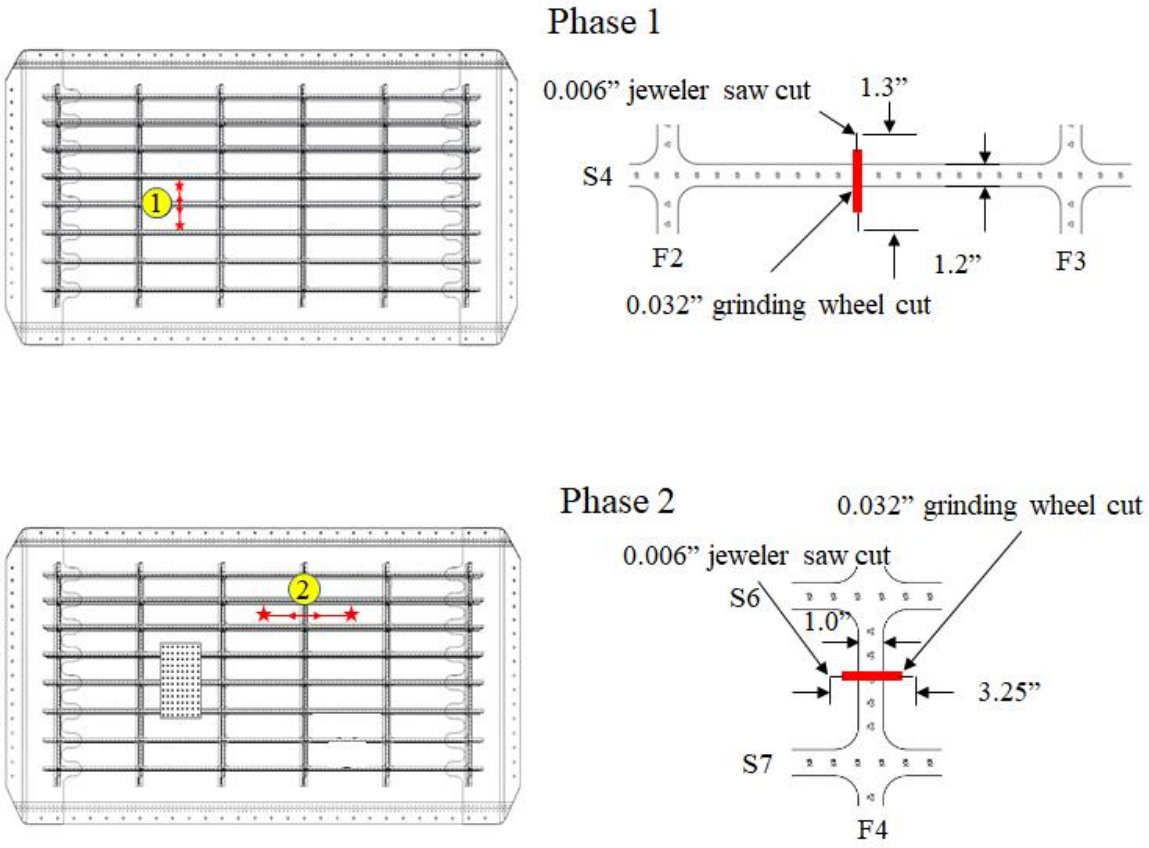

Figure 4. Initial damage scenarios used in the two test phases

2.3 Inspection and monitoring methods

During all phases of testing, several nondestructive inspection methods were used to monitor and record the formation and growth of cracks. Visual inspections were made on the inner and outer surfaces of the skin using high-magnification cameras that could be remotely controlled during the test. High-frequency eddy current was used on the outer surface of the skin. Along with these inspection methods, the baseline panel was instrumented with approx. 150 strain gages and digital image correlation (DIC) systems to monitor strains throughout the tests, as summarized in Appendices C and D, respectively. In addition, a commercial piezoelectric-based structural health monitoring system was used to collect data and to assess its capabilities to monitor FCG, highlighted in Appendix E.

2.4 Applied mechanical loads

The original goal of this program was to conduct different fuselage panel tests under the same loading conditions at a key location in the crown of a generic, single aisle commercial aircraft, where the loads are primarily due to pressure and bending from flight and landing loads. Damage tolerance performance was the key design criterion for both the longitudinal and circumferential directions. However, the panel 2 skin was approximately 18% thinner than panel 1 skin, due to small manufacturing tolerance difference in the chem-mill pocket thickness, which would have resulted in a significant difference in fatigue life using the same load conditions. The skin thickness difference in the "as-built" panel 2 was accounted for by testing panel 2 to the same stress intensity factors versus crack size as baseline panel 1 based on FEA. The test load conditions were adjusted using the finite element modeling (FEM) model results to match the stress intensity factor of panel 1 in order to have an "apple-to-apple" comparison of results between different panels.

The approximate applied stresses used in each test phase are shown in Table 3. Strain surveys were conducted at 75% of the fatigue loads. Fatigue loading was conducted using $R = 0.05$ and a frequency of 0.03 Hz. All testing was done under lab ambient conditions.

Table 3. Summary of applied stresses

Phase	**Test Type**	**Pressure (psi)**	**Axial Stress**		
			S_{eq} (ksi)	**S_{Press} (ksi)**	**$S_{axial\ 1g}$ (ksi)**
1	Strain Survey	7.425	9.20	4.52	4.53
	Fatigue	9.9	12.30	6.02	6.04
	Limit Load	9.9	25.88	6.02	7.94
2	Strain Survey	6.18	3.76	3.76	0
	Fatigue	8.24	5.01	5.01	0
	Residual Strength	14	8.51	8.51	0

3 Finite element analysis

Finite element analysis (FEA) for this program was originally conducted by Arconic, and the models were later transferred to the FAA.

In Phase 1 fatigue loads for panel 2, the pressure was kept the same as panel 1 at 9.9 psi. The ratio of hoop load and frame load was adjusted according to Flugge's solution (1952) for different As/Bt ratios (ratio between the area of stringer and the area of skin) due to the skin thickness and material property changes. The axial loads were adjusted to match the stress intensity factors between panel 1 and panel 2, as shown in Figure 5 (biased to the smaller crack sizes). Panel 2 phase 1 test loads are given in Figure 6 and Figure 7. Details of the analysis approaches used to develop test loads in this program are provided by Kulak et al. (2024)

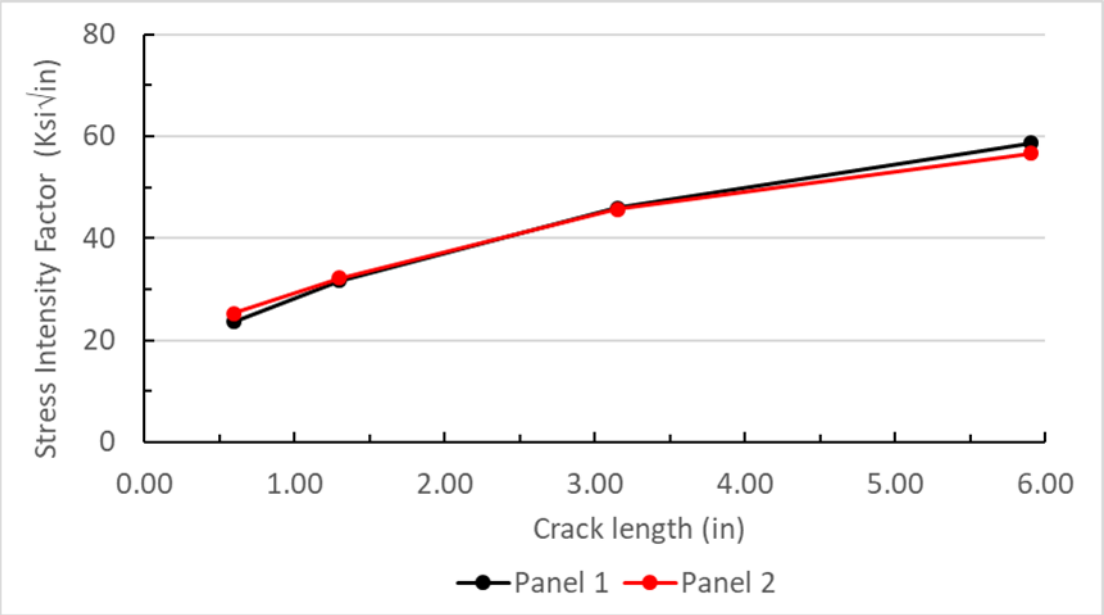

Figure 5. Phase 1 stress intensity factor comparison between panel 1 and panel 2

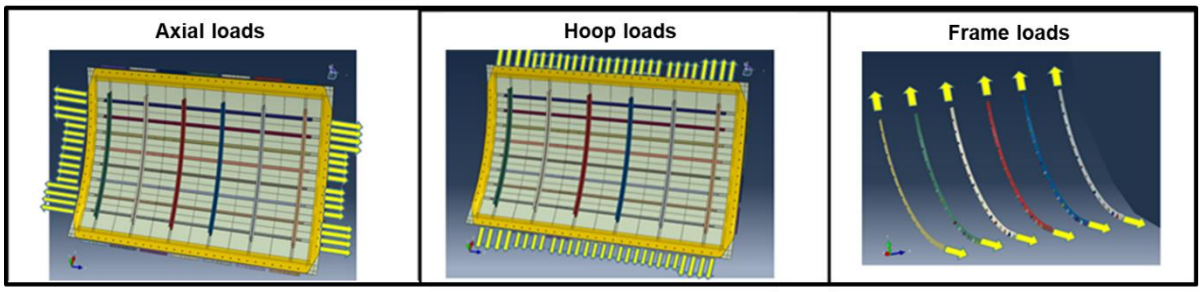

Skin Axial Actuator Load Arm Number	Applied Load (lbf)
1-4	17,738
5-8	11,126
9-12	11,126
13-16	17,738

Skin Hoop Actuator Load Arm Number	Applied Load (lbf)
1-4	10,458
5-8	9,729
9-12	9,500
13-16	9,408
17-20	9,500
21-24	9,729
25-28	10,458

Frame Number	Applied Load (lbf)
1	2,036
2	2,673
3	2,686
4	2,686
5	2,673
6	2,036

Figure 6. FASTER actuator loads for panel 2 Phase 1 fatigue test

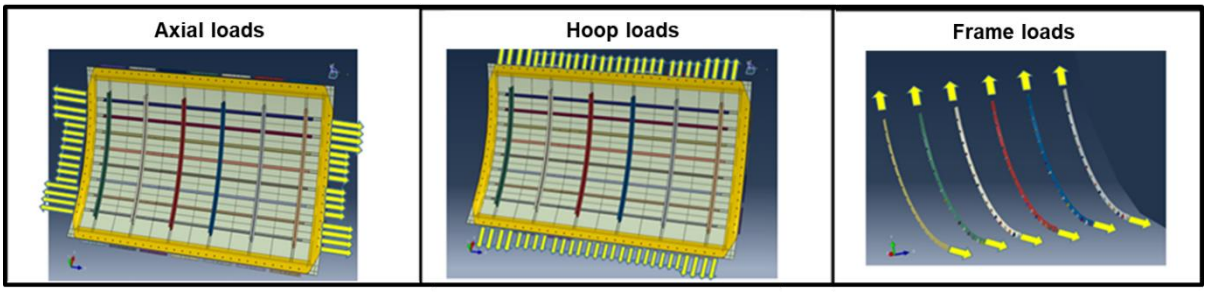

Skin Axial Actuator Load Arm Number	96% of target limit load (lbf)
1-4	37,019
5-8	23,220
9-12	23,220
13-16	37,019

Skin Hoop Actuator Load Arm Number	Applied Load (lbf)
1-4	10,458
5-8	9,729
9-12	9,500
13-16	9,408
17-20	9,500
21-24	9,729
25-28	10,458

Frame Number	Applied Load (lbf)
1	2,036
2	2,673
3	2,686
4	2,686
5	2,673
6	2,036

Figure 7. FASTER fixture actuator loads for phase 1 limit load

Phase 2 fatigue loads were determined by matching the panel 2 stress intensity factors to panel 1 phase 3 as-tested stress intensity factors versus crack length. The pressure was changed to 8.24 psi to produce the best match to the panel 1 phase 3 stress intensity factors. The axial loads used for the Phase 2 fatigue-crack growth test are shown in Figure 8.

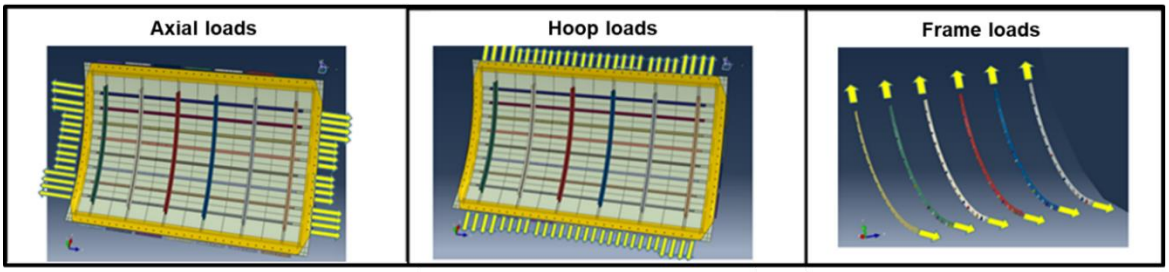

Skin Axial Actuator Load Arm Number	Applied Load (lbf)
1-4	6,740
5-8	4,213
9-12	4,213
13-16	6,740

Skin Hoop Actuator Load Arm Number	Applied Load (lbf)
1-4	8,708
5-8	8,101
9-12	7,910
13-16	7,833
17-20	7,910
21-24	8,101
25-28	8,708

Frame Number	Applied Load (lbf)
1	1,696
2	2,225
3	2,236
4	2,236
5	2,225
6	1,696

Figure 8. FASTER fixture actuator loads for Phase 2 fatigue test, pressure only

4 Results and discussion

Tests and analyses were performed to determine the fatigue and damage-tolerance performance of panel 2. The results from panel 2 will be used for comparison to the baseline panel 1 and future advanced fuselage panels with varying EMST. Representative results focus on panel 2 test for each phase.

4.1 Phase 1: two-bay circumferential notch with central stringer severed

4.1.1 Initial strain survey

A central crack-like notch was machined in the skin above the severed stringer S4, which is 1.30 in. total length and 0.032 in. wide. The notch was centered about the removed fastener, having the geometry shown in Figure 9. Initial strain surveys were conducted to verify proper load introduction to the baseline panel and validate the FEA model. Representative results shown in Figure 10 reveal that axial strains measured at gages near the original notch-tip were in agreement with FEA results.

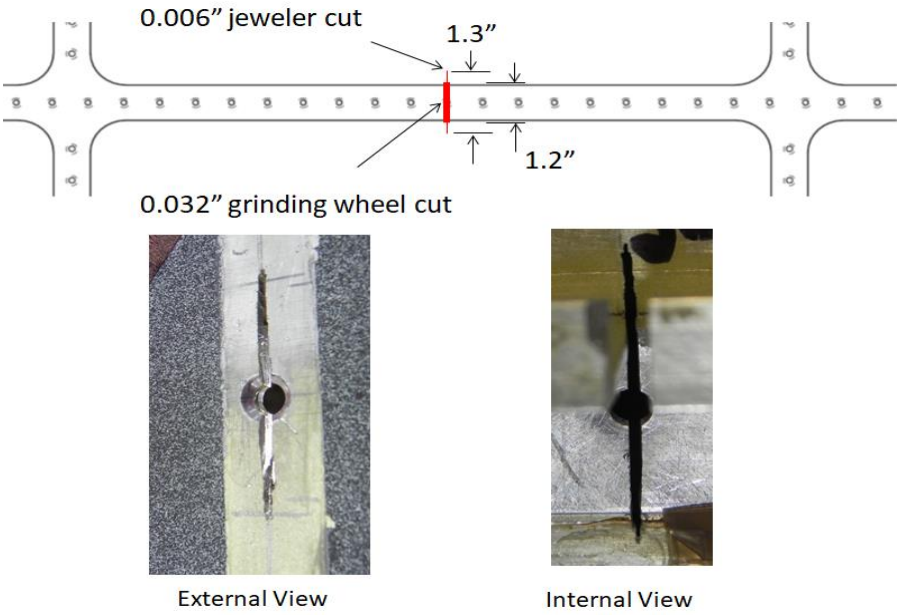

Figure 9. Configure of Phase 1 damage scenario

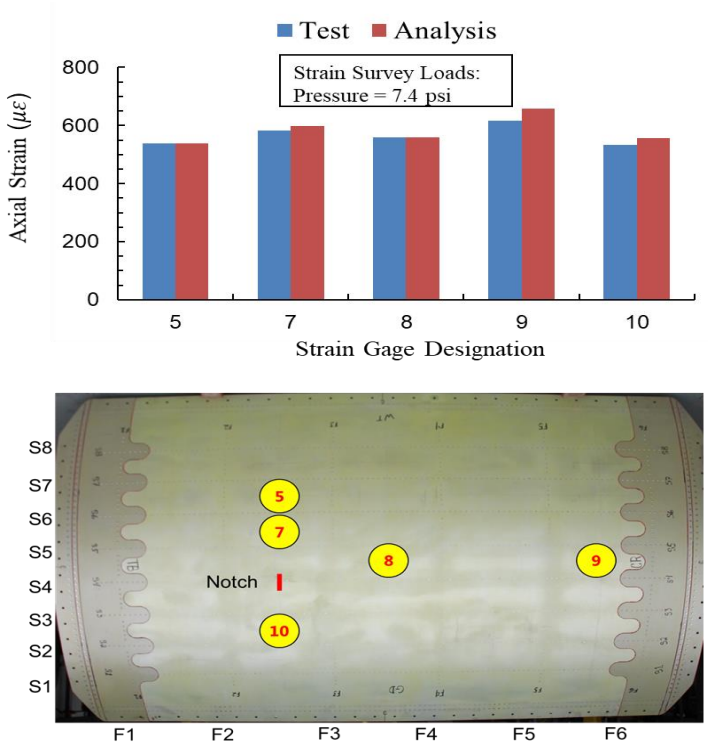

Figure 10. Phase 1 strain survey results verify FEA and applied

4.1.2 Fatigue test

The panel was fatigue tested under simulated flight load conditions for 48,850 cycles, during which the skin crack extended across two stringer bays to a final length of approximately 11 in., as shown in Figure 11 and Figure 12. In general, slow and stable crack growth was observed during the fatigue test. The crack surface morphology had distinct transition points where, on both sides, the surfaces changed from V (valley) to S (slant) fracture and from a +45° to a -45° slant fracture. Results indicate that crack-growth rates changed at these transition points similar to those observed in panel 1 testing (Tian, Stanley, & Backuckas, 2021) and coupon tests conducted on M(t) specimens (Stonaker, et al., 2019).

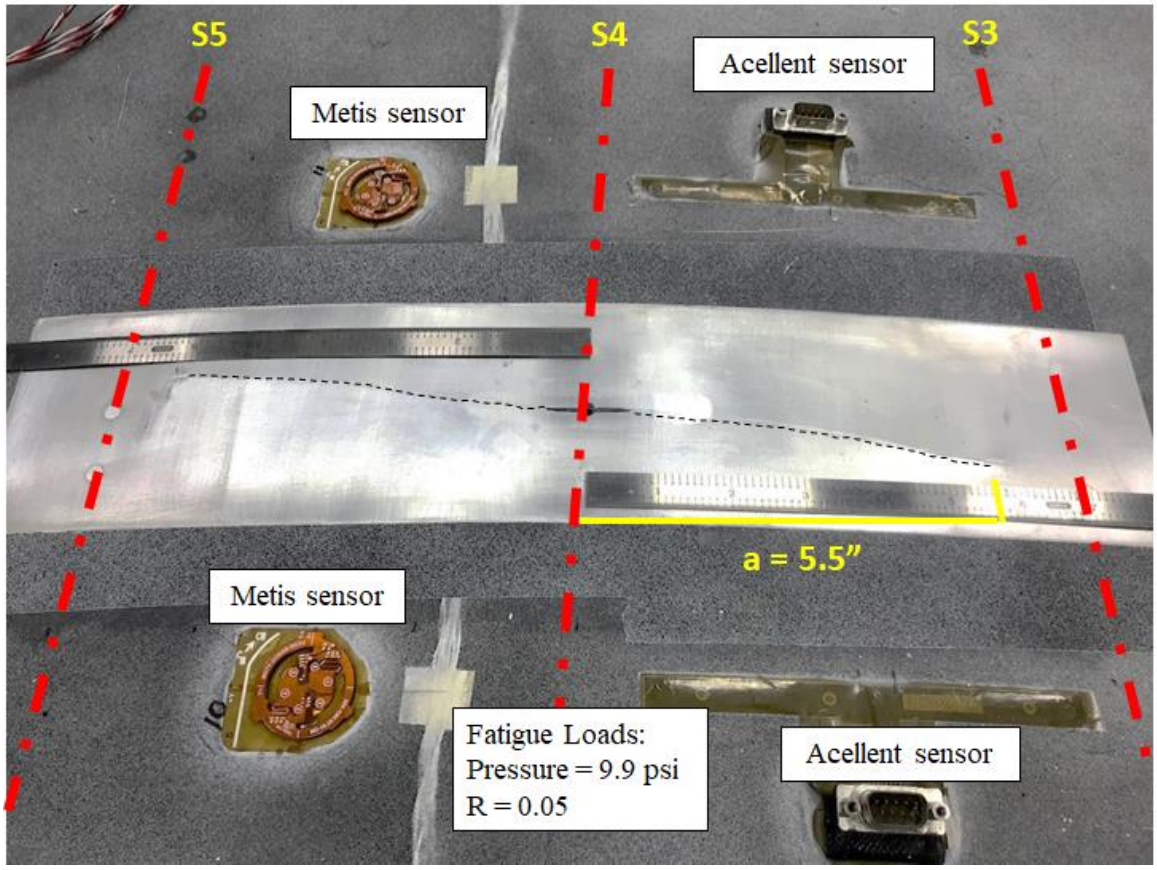

Figure 11. Picture of Phase 1 fatigue crack growth at 48,850 cycles

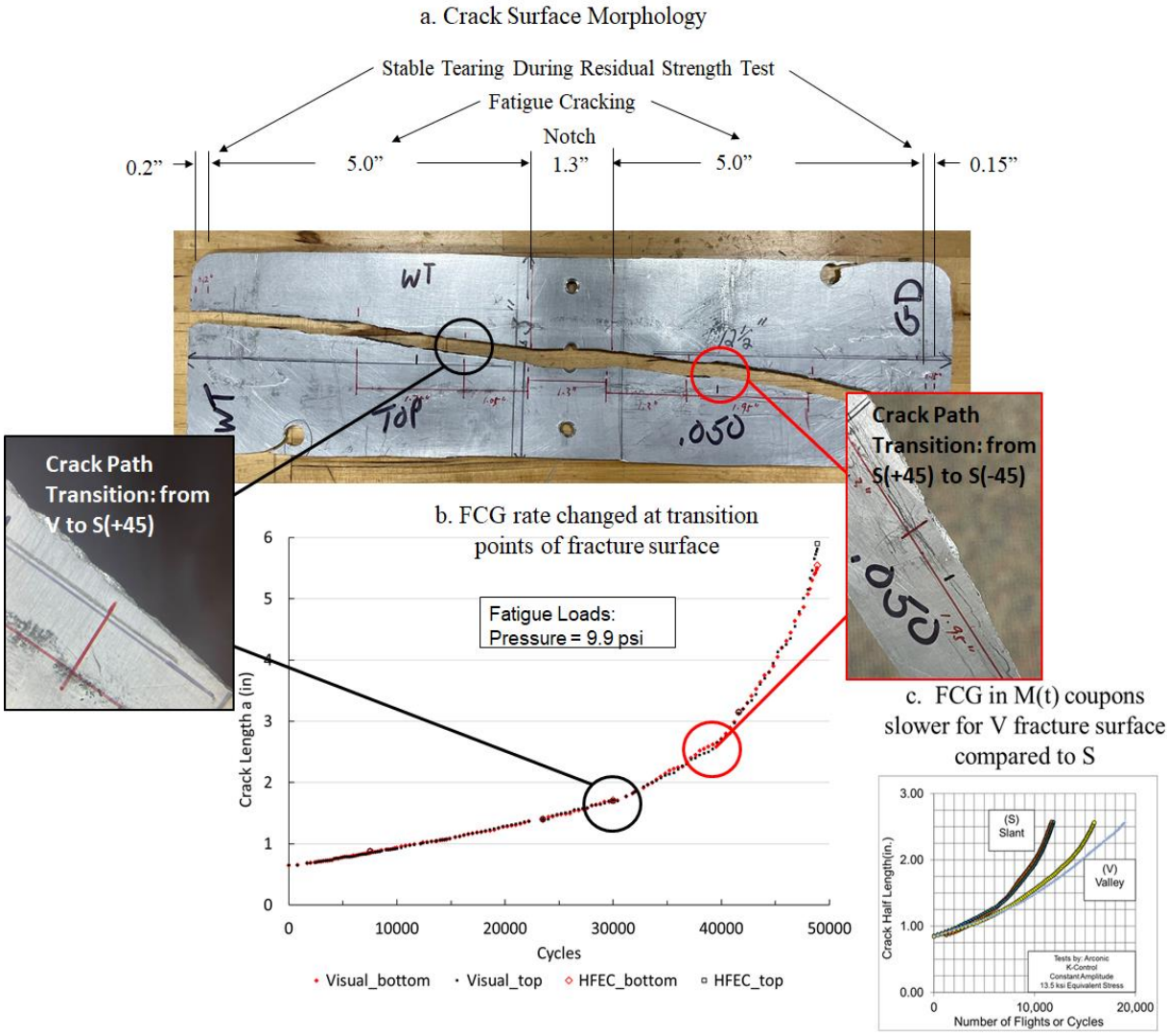

Figure 12. Phase 1 transition points of fracture surface morphology where FCG rates change

As shown in Figure 13, panel 2 exhibited better fatigue crack growth performance compared to panel 1. Crack extension occurred across two stringer bays to a final length of about 11 inches after 33,600 and 48,850 fatigue cycles in panel 1 and 2, respectively.

Strain surveys were conducted during the fatigue test at same crack length as panel 1 (panel 1 strain survey was conducted at 3000 cycle intervals). The far-field axial strains in the mid-bay regions remained relatively constant throughout the fatigue test. Slight strain redistribution was evident after 30,000 cycles due to the crack extension, as shown in Figure 14. Strains increased in gages 7 and 10, as the crack grew closer to those gages. In addition, strains in gage 8 reduced due to crack shielding.

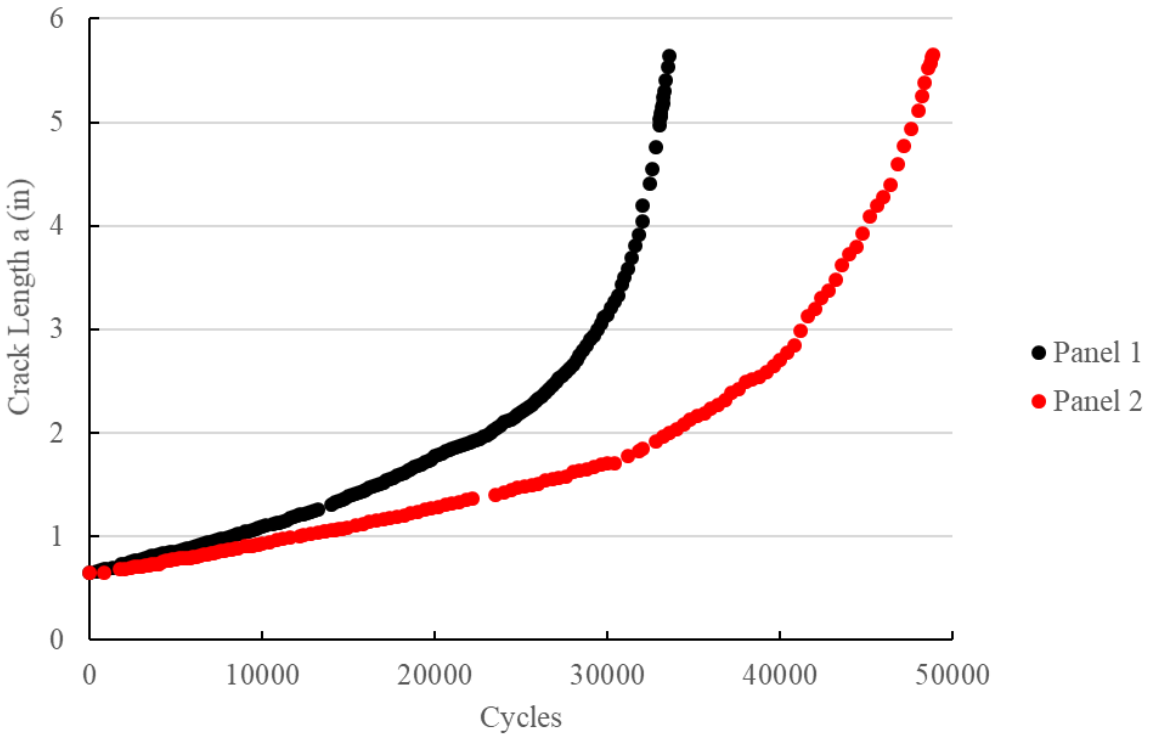

Figure 13. Circumferential crack growth comparison between panel 1 and panel 2

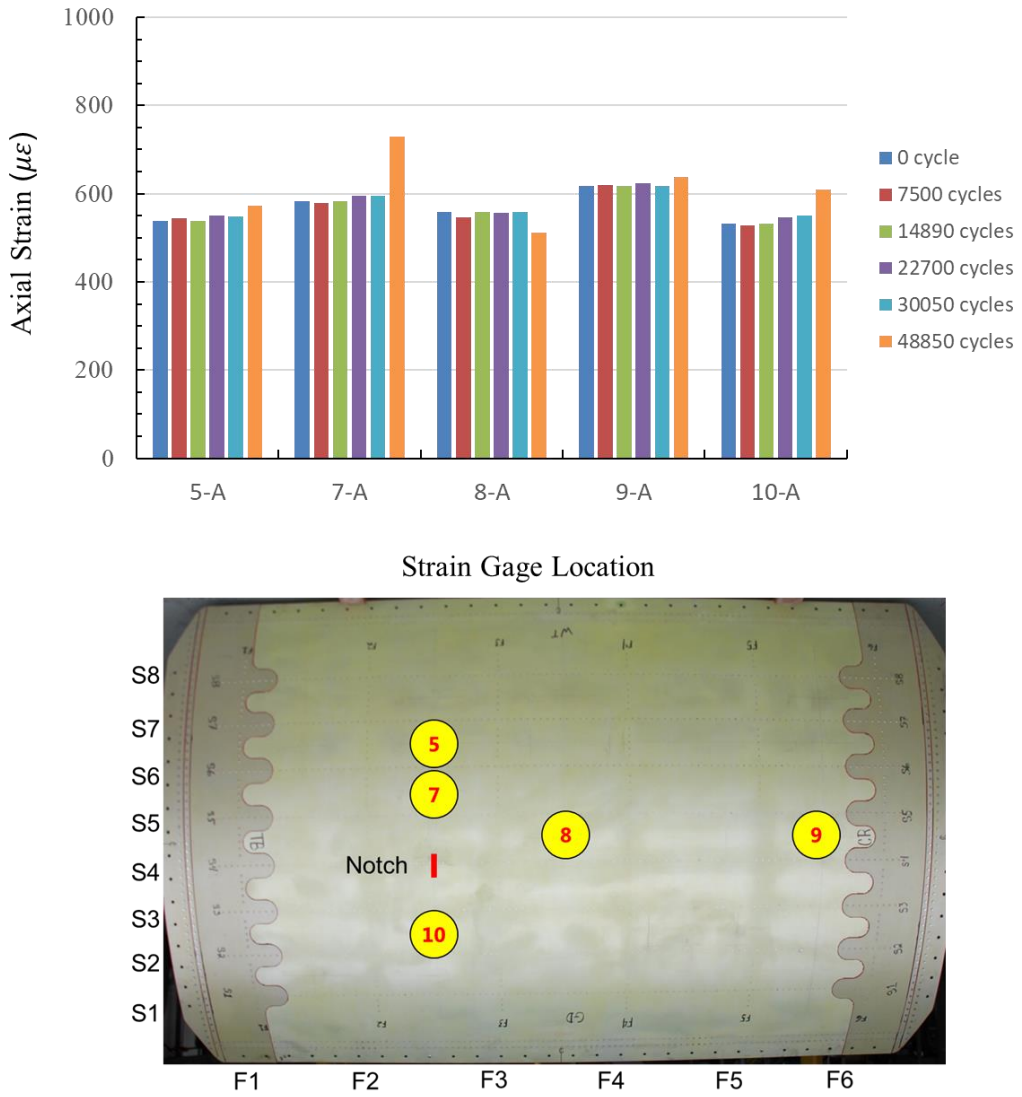

Figure 14. Far-field axial strain distribution measured in skin mid-bay regions during the fatigue test

Local to the crack, strain redistribution was more significant on internal local skin and stringer gages, as shown in Figure 15 and Figure 16 respectively. The magnitude of strain increased as the crack tip approached the gages. As the crack grew past the gages, strains in the skin subsequently reduced.

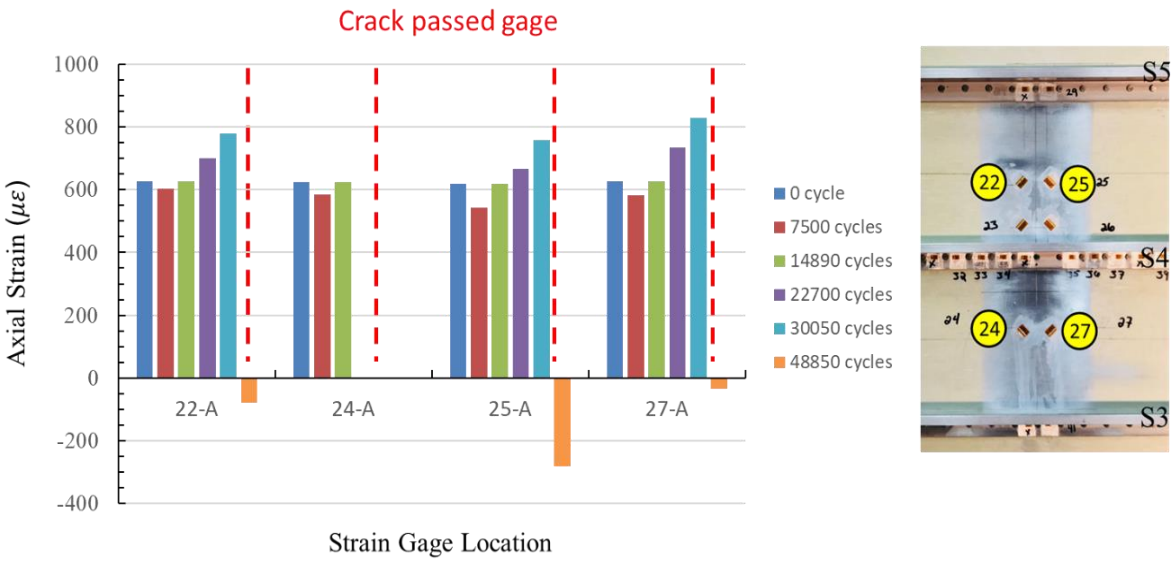

Figure 15. Representative strain survey results for Phase 1 internal skin rosette gages

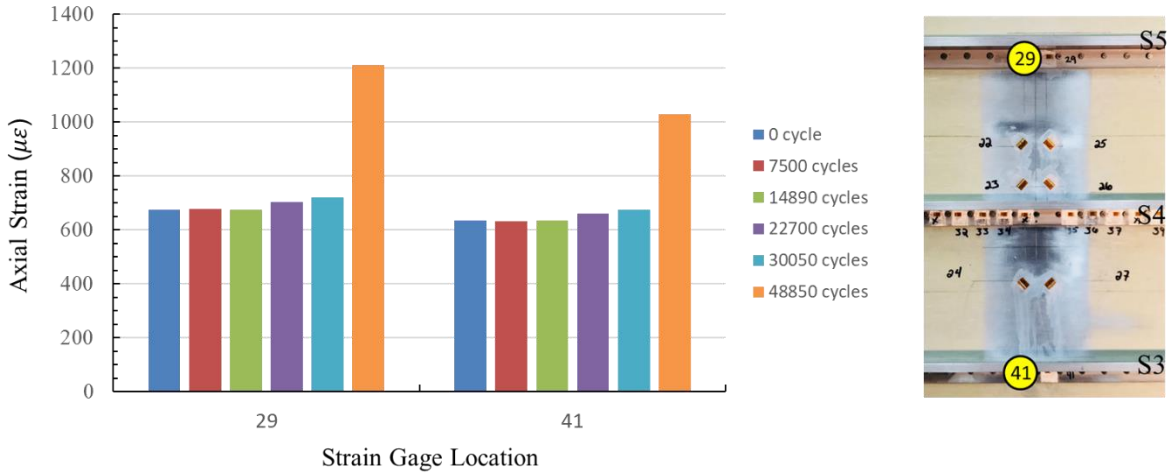

Figure 16. Representative strain survey results for Phase 1 stringer gages

4.1.3 Limit load test

After fatigue testing, panel 2 was subjected to approximately 2.5 g of axial load in a limit load test holding the pressure constant at 9.9 psi. Strain gages located on the inner and outer flanges of the stringer ahead of the fatigue crack revealed that the stresses were below the yield strength of the stringer material (see Figure 17). The intact stringers ahead of the crack were effective in containing the damage. In addition, limited stable-tearing extension and crack-tip plasticity was observed from each crack tip, as shown in Figure 18 using DIC measurements.

The panel was then repaired for follow-on phases, as shown in Appendix B. The strain survey was conducted to ensure there is no effect of repair on Phase 2 test bay, as shown in Figure 19.

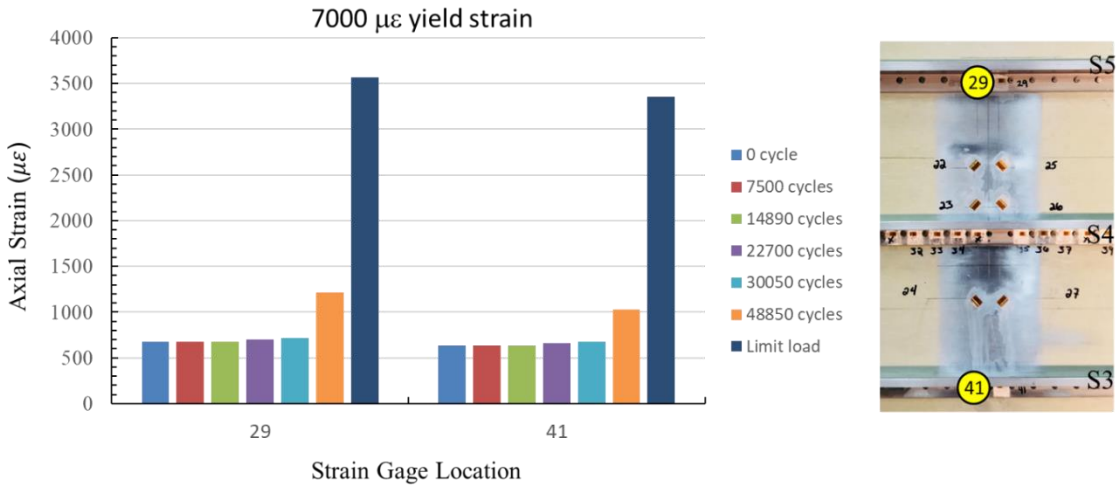

Figure 17. The result of stringer gages during the circumferential direction limit load test

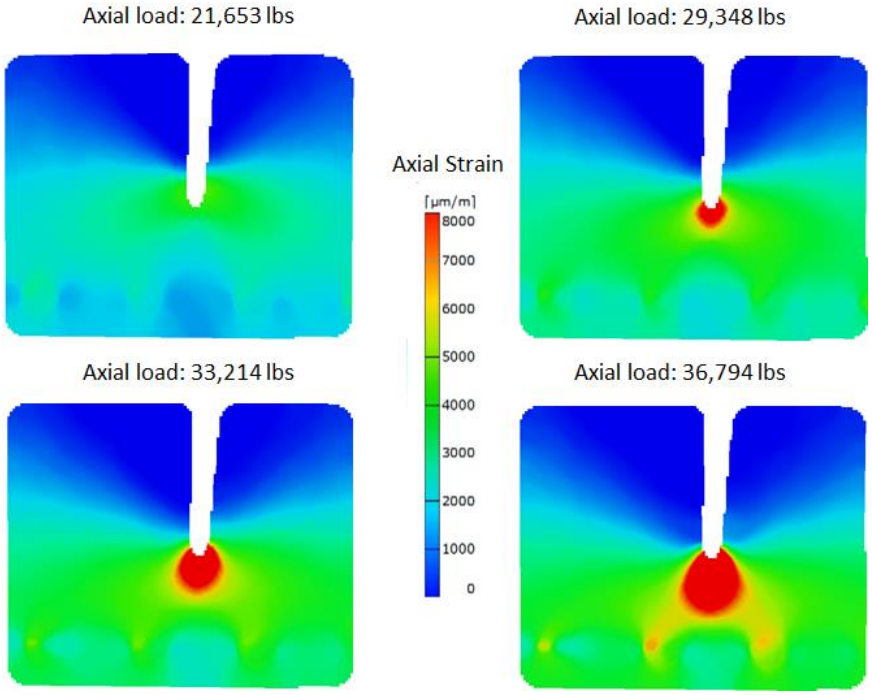

Figure 18. ARAMIS result during the circumferential direction limit load test

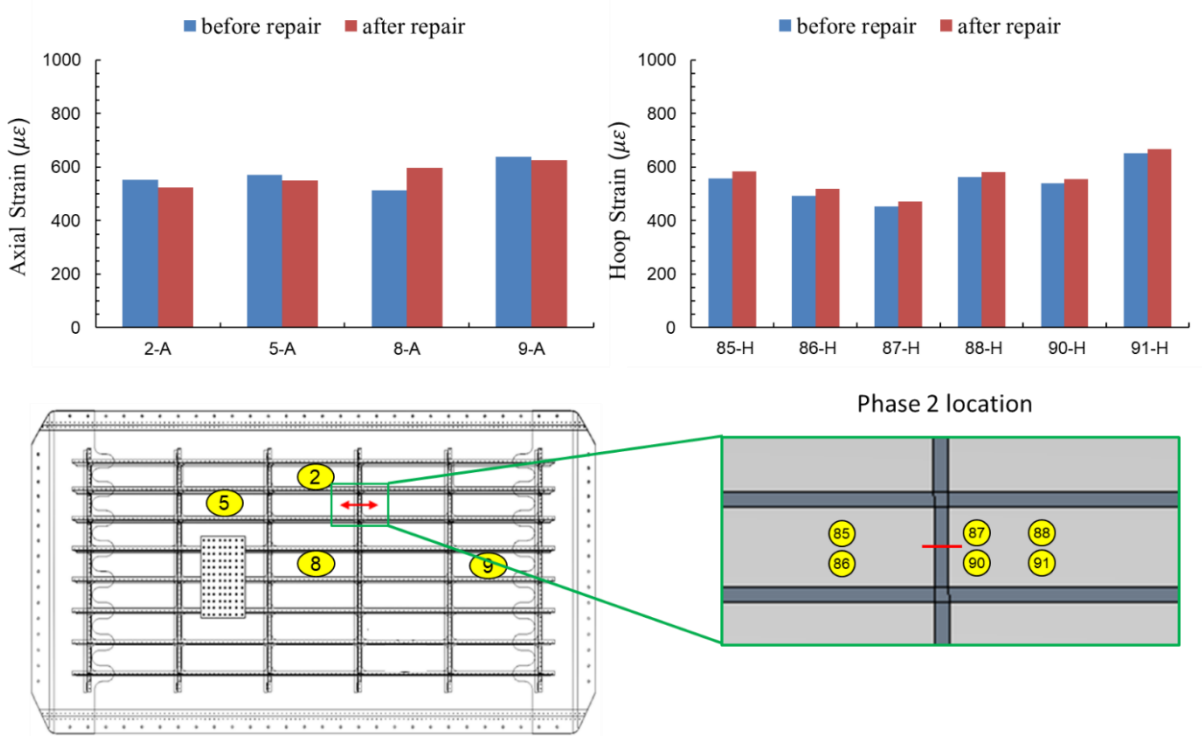

Figure 19. Strain survey after Phase 1 crack repair

4.2 Phase 2: Two-bay longitudinal notch with central frame severed

The longitudinal damage scenario for Phase 2 is shown in Figure 20.The frame F4 rivet at the mid-frame location between stringers S6 and S7 was removed, and frame F4 was severed at this location. Damage was simulated by machining a 3.25-in. long notch in the skin above the severed F4 frame.

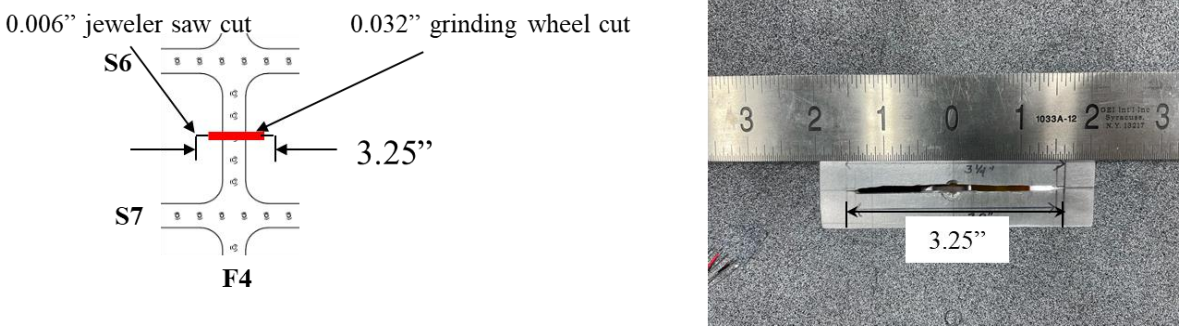

Figure 20. Configuration of Phase 2 damage scenario

For this phase, the panel was fatigue tested under pressure load conditions for 37,070 cycles, during which the skin crack extended across two frame bays to a final total length of approximately 16 in. The crack growth was non-symmetrical as shown in solid lines in Figure 21. The fatigue test phase ended at 36,700 cycles, when the right side crack was about 5.4”. The left side crack was extended using a grinding wheel to the same length as the right side. Then, the panel was fatigue cycled under the same pressure load conditions for about 800 cycles so that panel 2 has the same total crack length as panel 1 for the residual strength test.

Post-residual strength test investigation revealed that the unsymmetrical crack growth was due to the transition of crack surface morphology resulting in crack growth-rate changes as observed during Phase 1 fatigue test. The right-side crack had slanted crack surface and transitioned back and forth from +45 to -45 at approximately 24,600 cycles (1.8” crack extension), 28,600 cycles (2.24” crack extension) and 33,400 cycles (3.0” crack extension) respectively. The left side crack had slant crack surface up to 0.75” and changed to V surface for the rest of the fatigue cycles, which led to the slower crack grow. However, panel 2 exhibited better average crack growth performance compared to panel 1, as shown in Figure 22. Crack extension occurred across two frame bays to a final length of about 15.25 inches after 29,000 and 37,070 fatigue cycles in panel 1 and 2, respectively.

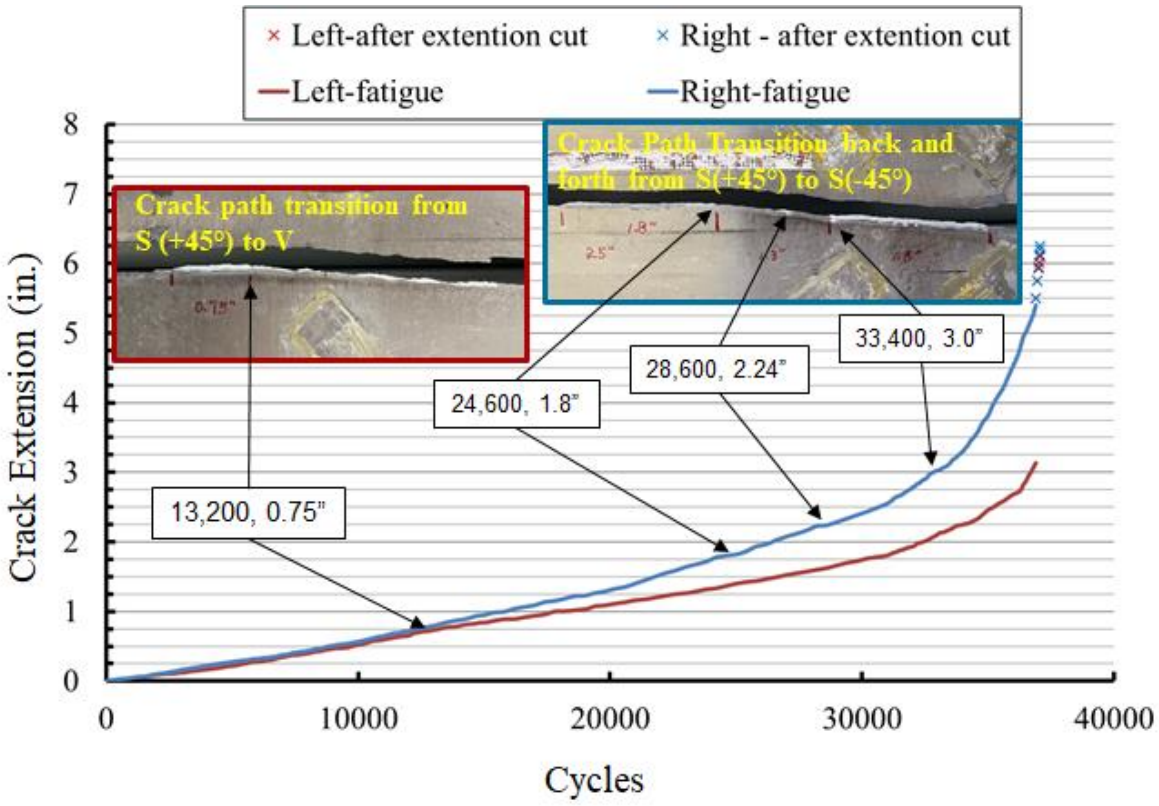

Figure 21. Slow and nonsymmetrical fatigue crack growth

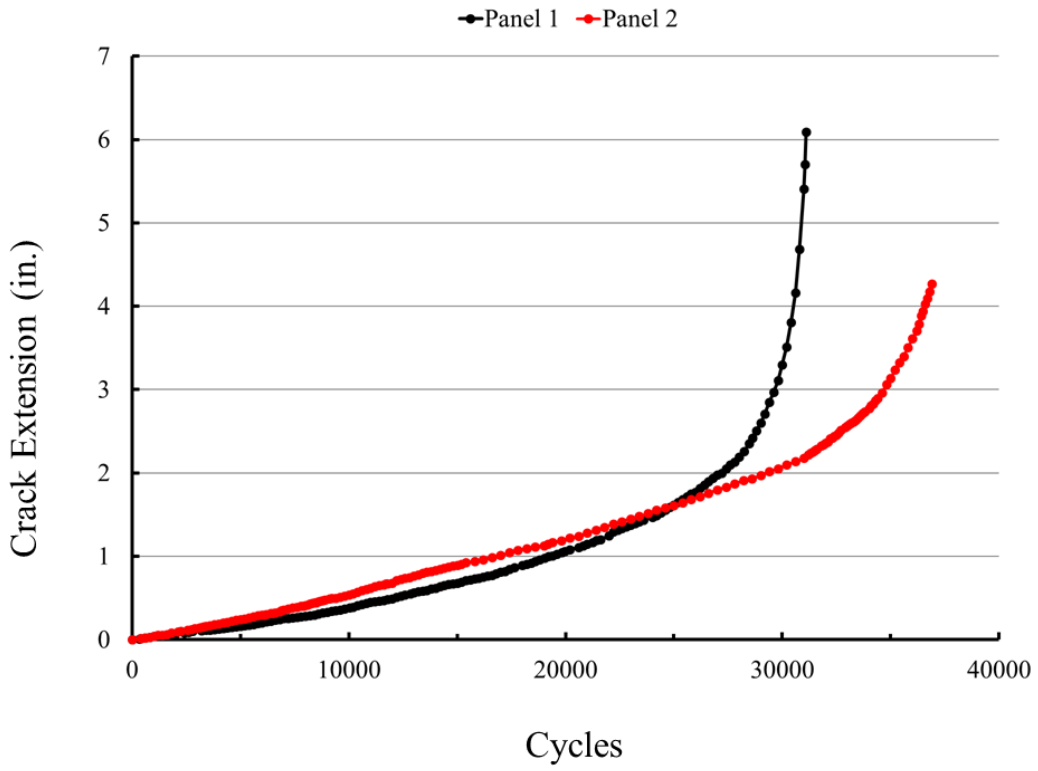

Figure 22. Average longitudinal crack growth comparison between panel 1 and panel 2

After fatigue testing, the final stage of testing is a residual strength test to certain limit load conditions identified in 14 CFR §25.571 (b) (Damage-tolerance... , 2023). The residual strength test was conducted under pressure loading applied quasi-statically. Unstable tearing occurred at maximum applied pressure of 14 psi, resulting in failure of the panel. Extensive damage occurred to the panel where the skin crack extended to a total length of 100 inches and severed two intact frames, as shown in Figure 23. The pressure at failure exceeded the residual strength damage-tolerance requirements in 14 CFR §25.571 (b).

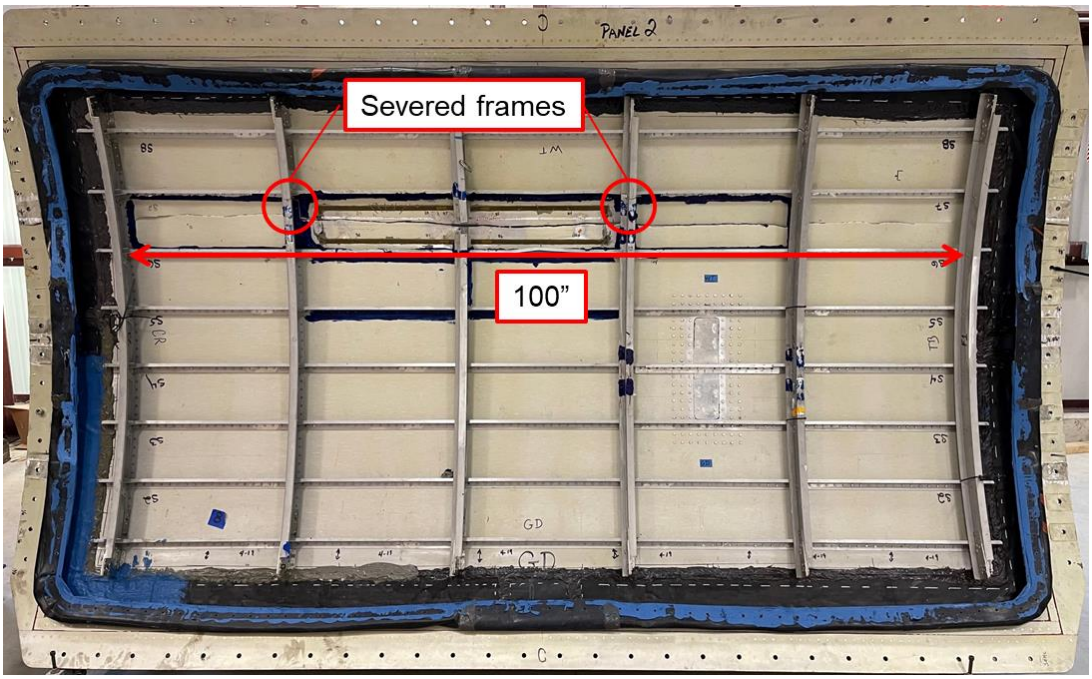

Figure 23. Picture of panel 2 after residual strength test

5 Summary

In a collaborative effort, the FAA, Arconic, and Embraer are assessing emerging metallic structures technologies (EMST) for fuselage applications through full-scale test and analysis. Several technologies are being considered, including advanced aluminum-lithium alloys and selective reinforcement using fiber metal laminates. Data from this study will be used to verify potential improved damage-tolerance performance and structural safety potential that EMST offer compared to the current fuselage structure constructed with conventional materials and fabrication processes, with a goal to provide guidance when considering EMST. This report documented results from panel 2 tests subjected to two phases of testing and accumulated 85,920 simulated flights.

Results from the panel 2 test will be compared to with the first baseline panel 1 and future tests on advanced panels containing varying EMST. Results and other major findings include:

- **Phase 1**: A two-bay circumferential crack-like notch having a total length of 1.3 in. was machined in the skin with the central stringer severed. The panel was then subjected to 48,850 fatigue cycles, during which slow and stable crack growth occurred to a final length of 11.3 in. Afterwards, a limit load test was conducted in which the panel was subjected to approximately 2.5 g axial load under a constant operational pressure level.

Limited stable tearing extension was observed from each crack-tip. Panel 2 exhibited approximately 45% improvement in fatigue life compared to the baseline panel 1 for the circumferential damage scenario.

- **Phase 2**: A two-bay longitudinal crack-like notch was machined in the skin having a total length of 3.25 in. with the central frame severed. After 37,070 cycles of fatigue testing, the skin crack extended approximately to a total length of 15 in. Compared to the baseline panel 1, panel 2 exhibited approximately 21% improvement in fatigue life for this damage scenario. During the subsequent residual strength test, the panel failed at 14 psi pressure. This pressure exceeded the residual strength damage-tolerance requirements defined in 14 CFR §25.571 (b) (Damage-tolerance... , 2023).

6 References

Bertoni, M., Fernandez, F., & Miyazaki, M. (2014). Fuselage technology demonstrator. *Proceedings of AeroMat 2014.* Orlando, FL.

Beumler, T. (2014). Development of thin-walled FML-structures. *Proceedings of AeroMat 2014.* Orlando, FL.

Chaves, C. (2017). A review of aeronautical fatigue investigations in Brazil. *Proceedings of the 35th ICAF Conference.* Nagoya, Japan.

Damage-tolerance and fatigue evaluation of structure, 14 CFR § 25.571 (2023). Retrieved from https://www.govregs.com/regulations/14/25.571

Eberl, F., Smith, P., Layel, J., Fernandez, F., Nunes, D., Cruz, M., . . . Garcia, J. (2015). Manufacturing of a novel upper wing cover demonstrator using friction stir welding. *Proceedings of AeroMat 2015.* Long Beach, CA.

Flugge, W. (1952). *Stress problems in pressurized cabins.* NACA Technical Note.

Heinimann, M., Kulak, M., Bucci, R., James, M., Wilson, G., Brockenbrough, J., . . . Sklyut, H. (2007). Validations of advanced metallic hybrid concepts with improved damage tolerance capabilities for next generation lower wing and fuselage applications. *Proceedings of the 24th ICAF Symposium.* Naples, Italy.

Kok, L., Poston, K., & Moore, G. (2011). Bombardier aerospace FSW demonstrator. *Proceedings of the 26th ICAF Symposium.* Montreal, Canada.

Kulak, M., Bakuckas, J, Tian, Y., Stanley, D., Chang, P., & Sklyut, H. (2024). *Design, analysis and test development of full-scale fuselage test panels to assess emerging metallic structures technologies [DOT/FAA/TC-24/1].* Federal Aviation Administration.

Lowak, H., de Jonge, J., Franz, T., & Schutz, D. (1979). *MINITWIST - A shortened version of TWIST.* NLR Report No. TB-146.

Prasad, N., Gokhale, A., & Wanhill, R. (. (2014). *Aluminum-lithium alloys, Processing, properties, and applications.* Elsevier.

Schmidt, H. (2005). Damage tolerance technology for current and future aircraft structure. *Proceedings of the 23rd ICAF Symposium.* Hamburg, Germany.

Silva, D., Cruz, M., Menonca, W., Brandao, F., Sakata, A., Silva, G., & Kulak, M. (2017). Manufacturing of a fiber metal laminate lower wing cover demonstrator. *Proceedings of AeroMat, 2017.* Charleston, SC.

Steadman, D. (2007). *Destructive evaluation and extended fatigue testing of retired transport aircraft [DOT/FAA/AR-07/22 V5]*. Volume 5: Data Analysis Report. Federal Aviation Administration.

Stonaker, K., Bakucka, W. I., & Freisthler, M. (2015). Material characterization of aluminum lithium alloys used in aerospace applications. *Proceedings of the 28th ICAF Symposium.* Helsinki, Finland.

Stonaker, K., Bakuckas, J., Stanley, D., Kulak, M., Chang, P., & Freisthler, M. (2019). Assessment of fatigue behavior of advanced aluminum alloys under complex variable amplitude loading. *Proceedings of the 30th ICAF Symposium.* Krakow, Poland.

Tian, Y., & Backuckas, J. (2019). *Full-scale aircraft structural test evaluation and research (FASTER) fixture [DOT/FAA/TC-TN19/6]*. Federal Aviation Administration.

Tian, Y., Stanley, D., & Backuckas, J. (2021). *Assessment of emerging metallic structures technologies through test and analysis of fuselage structure: Test panel 1. [DOT/ FAA/TC-21/25]* [Federal Aviation Administration.

A Panel 2 geometry

The skin, frame and stringer geometry described in this Appendix were selected from a crown location forward of the wing centerline. At this location, the panel geometry was equally critical for crack growth circumferentially and longitudinally, and the same geometry would be relevant for axial and longitudinal loading.

The materials in the baseline Panel 2 are described in Table 2. The geometry was determined using the sizing methods described by Kulak (2024) using the materials in Table 2.

The overall panel design is shown in Figure A-1. The panel length is approximately 125 in., and the length of the panel arc is 76.5 in. with a vertical projection of 73.2 in.

Engineering drawings for Panel 2 construction are included below.

Fuselage Skin Sheets

The fuselage skin for the baseline panel 2 utilized a 2060-T8 sheet. The skin was supplied in a gage of 0.09 in. and was bare sheet. The final skin thickness in the stringer and frame attachment landings was 0.065 in., and the skin was pocketed to 0.050 in. (see Figure A-2). The rivets on the

airflow side of the fuselage panels for the skins, stiffeners, and frames were the 100-degree countersunk fastener NAS1097AD-5, which has a 5/32-in. diameter (AD = 2117-T4 rivet). For the stringer clips in panel 2 the universal head rivet MS20470AD-5 (5/32-in. diameter, 2117-T4) was used.

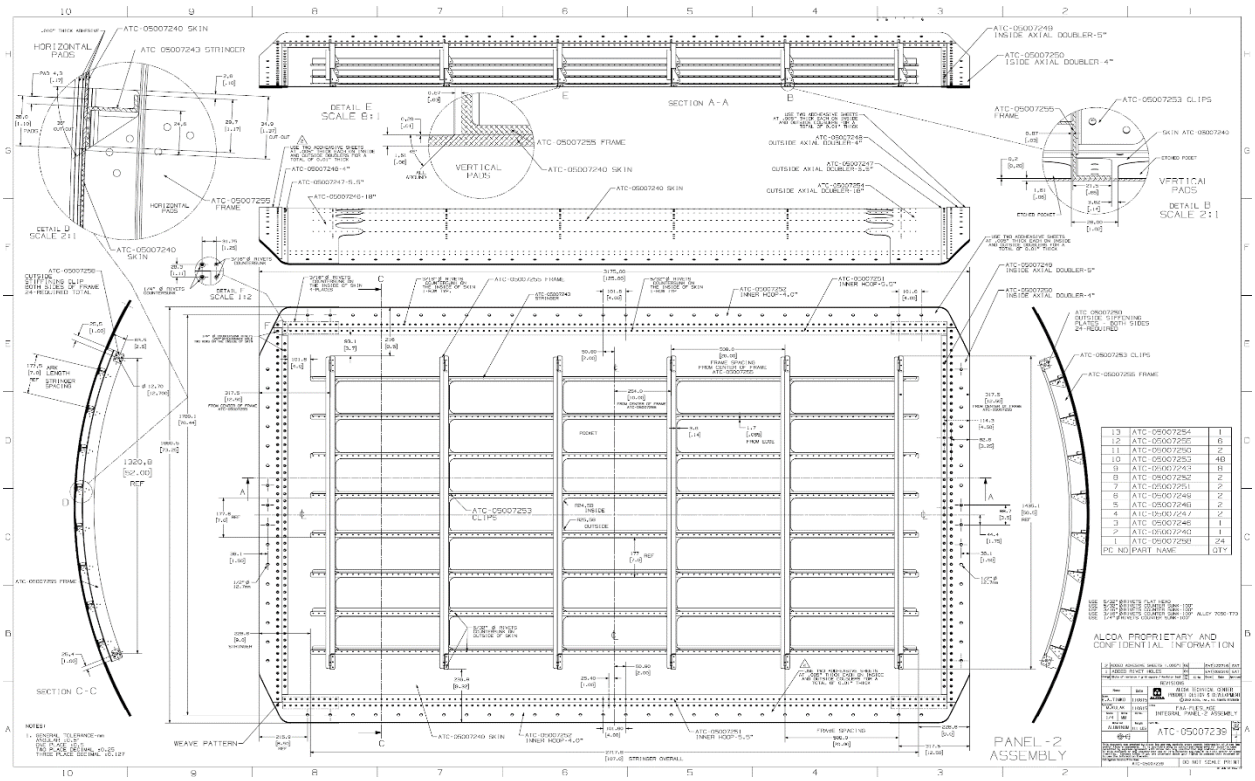

Figure A-1. Panel 2 overall dimensions

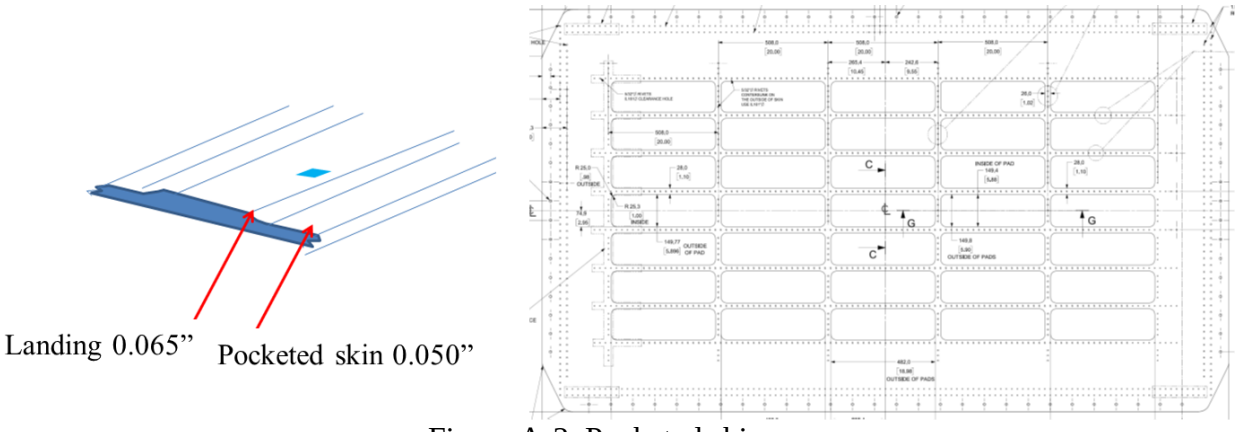

Figure A-2. Pocketed skin

Panel 2 Load Introduction Doublers and Bonding to Skins

For panel doublers, a higher-strength 7xxx sheet, like 7075-T6, was used (non-clad). The edge doublers package on both the inside and outside of the fuselage panel were roll formed to curvature. The doubler package was prepared for bonding to the skins.

The doublers were bonded to the skin, using either an oven-cured epoxy like FM73 or a cold bonding adhesive. In addition, countersunk Huck bolt or Lock bolt fasteners were used to secure all edge doublers.

After chemical milling, the panel underwent the appropriate surface treatment procedure—in stringer frame landings and pocketed regions—to protect the panel against corrosion and allow sealant to be used under the frame and stringer areas, which are riveted to the skin. After chemical milling, the pocketed regions were anodized and primed.

Stringer clip

The frame system for Panel 2 utilized a one-piece integral frame construction, where the integral frame is attached to the skin directly and to stringer via a stringer clip, as shown in Figure A-3. The stringer clip used 7075-T62.

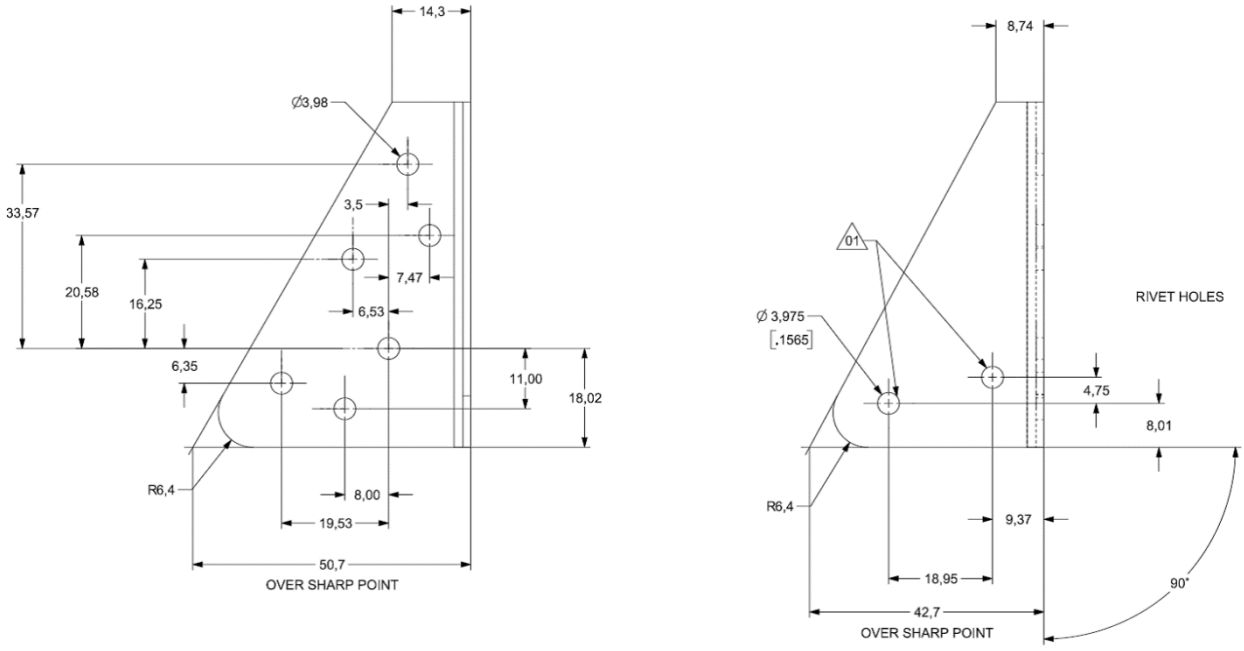

Figure A-3. Stringer clip

Frame

The frame, as shown in Figure A-4 was riveted directly to the skin and stringer through stringer clips using the previously identified fasteners. The frame was made of 2099-T83 extrusions alloy. The frame was stretch formed to a constant radius reflecting the offset from the skin radius.

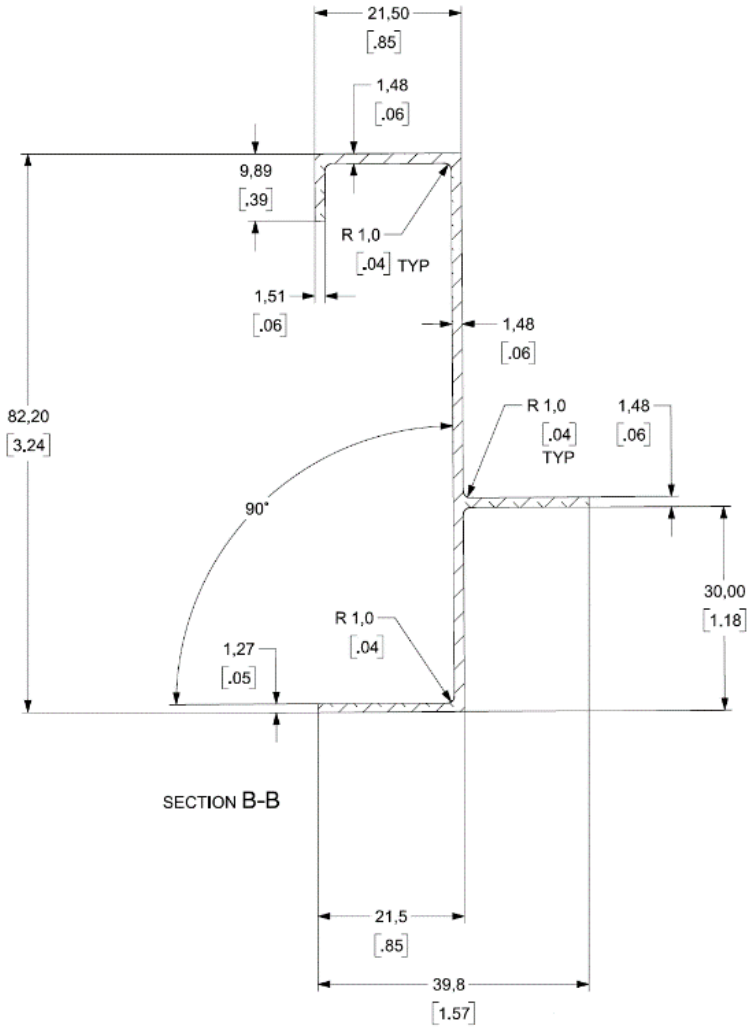

Figure A-4. Frame

Stringer

The stringers were made of 2055-T84 extrusions. The Z cross-section was extruded with attach flanges of a radius to match the 74-inch-radius curve of the panel, as shown in Figure A-5.

Loading and doublers

The test panel was loaded through the skin by actuators axially and in the hoop direction. The frames were also loaded in the hoop direction at each frame end by individual actuators. The test panel was loaded internally by pressure. See panel 1 report for details of doublers at panel edges and frame end load attachment points (Tian et al., 2021).

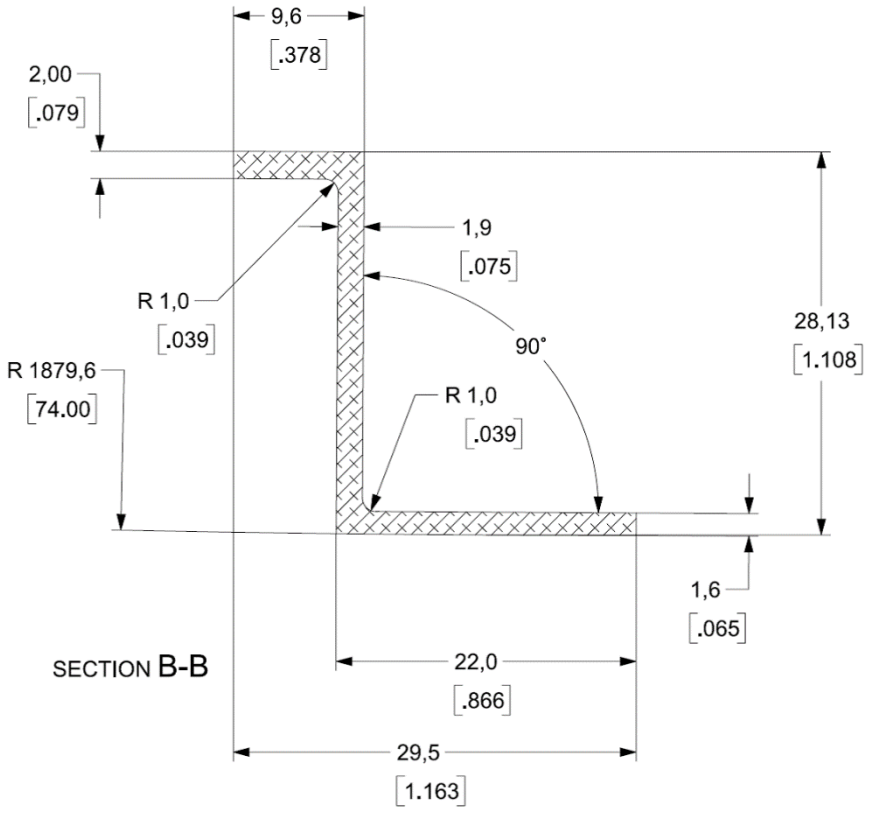

Figure A-5. Stringer

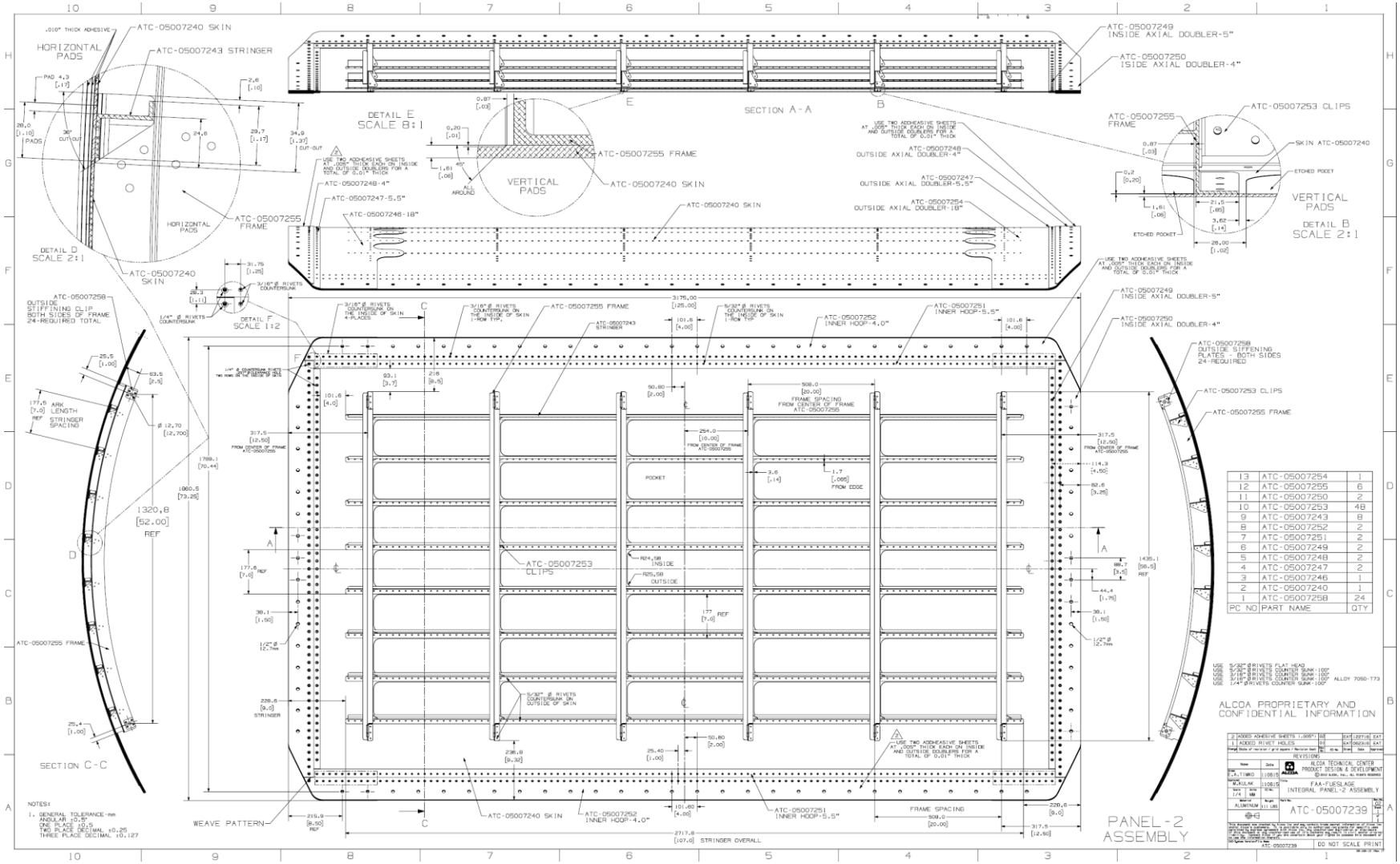

Figure A-6. Panel 2 assembly drawing

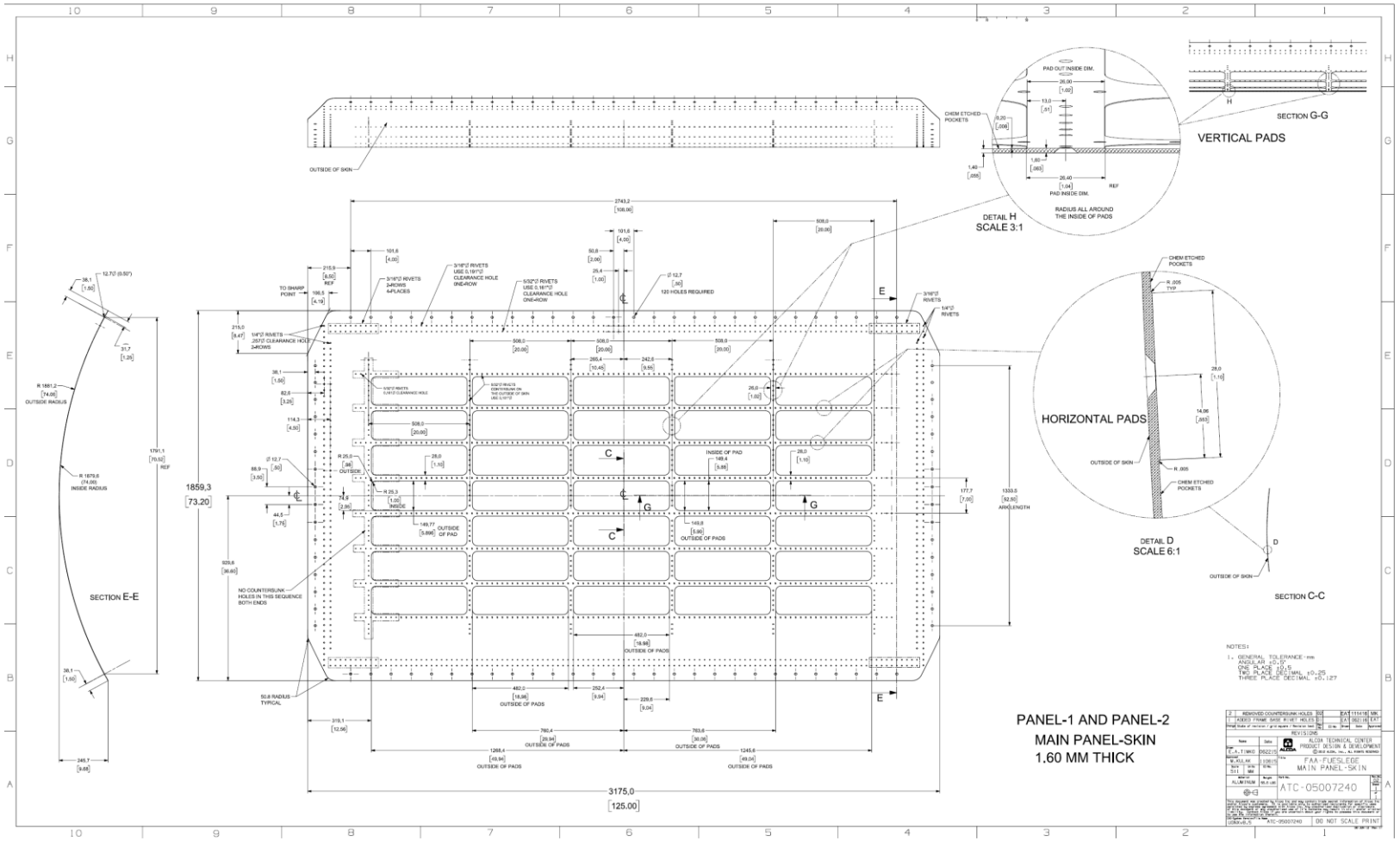

Figure A-7. Panel 2 skin

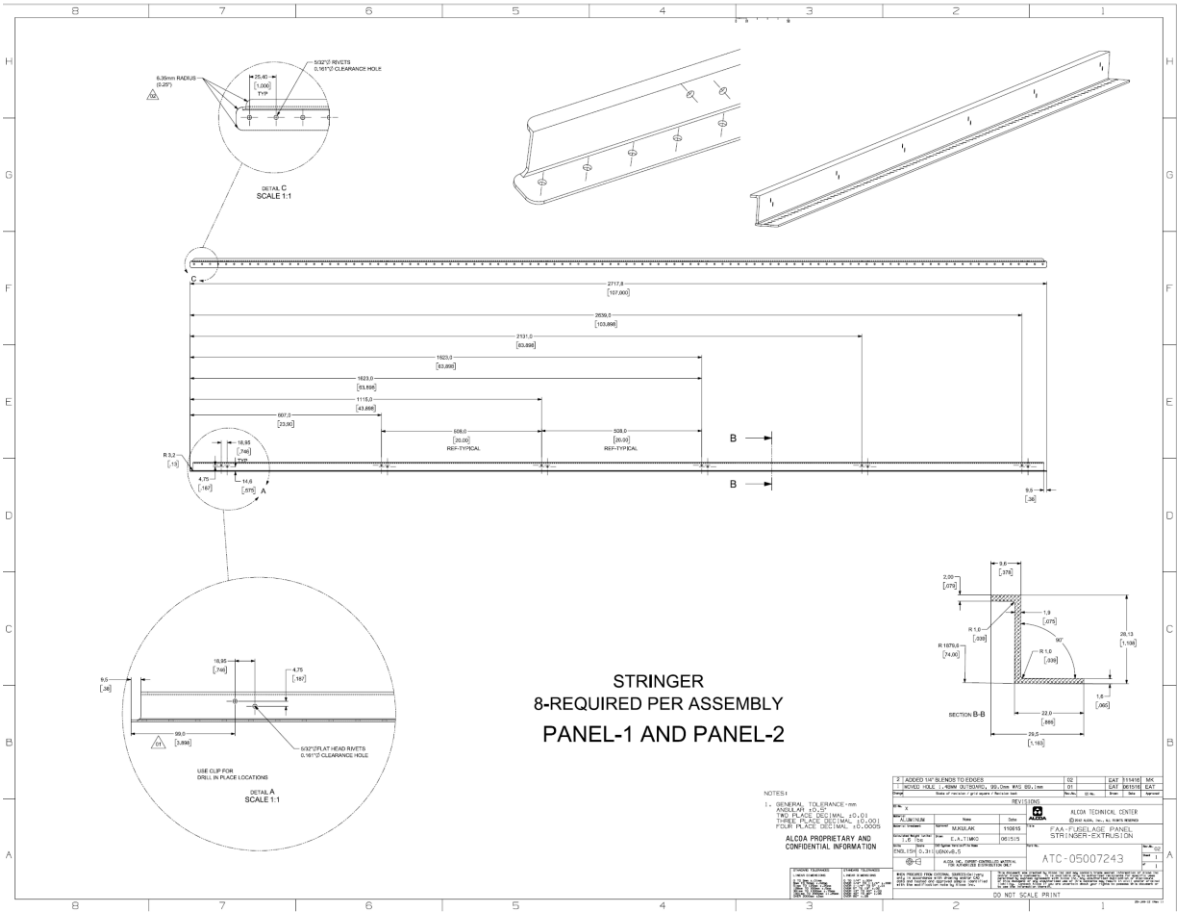

Figure A-8. Panel 2 stringer

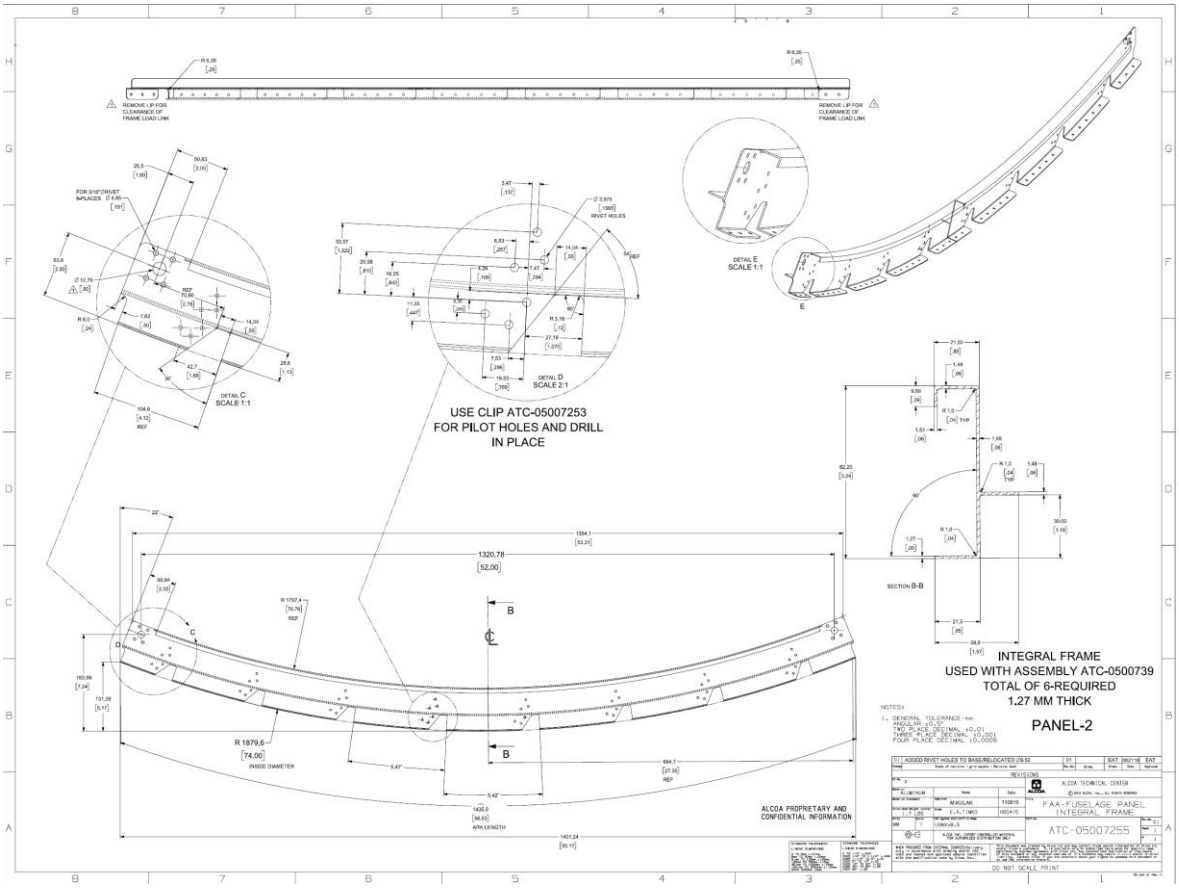

Figure A-9. Panel 2 frame

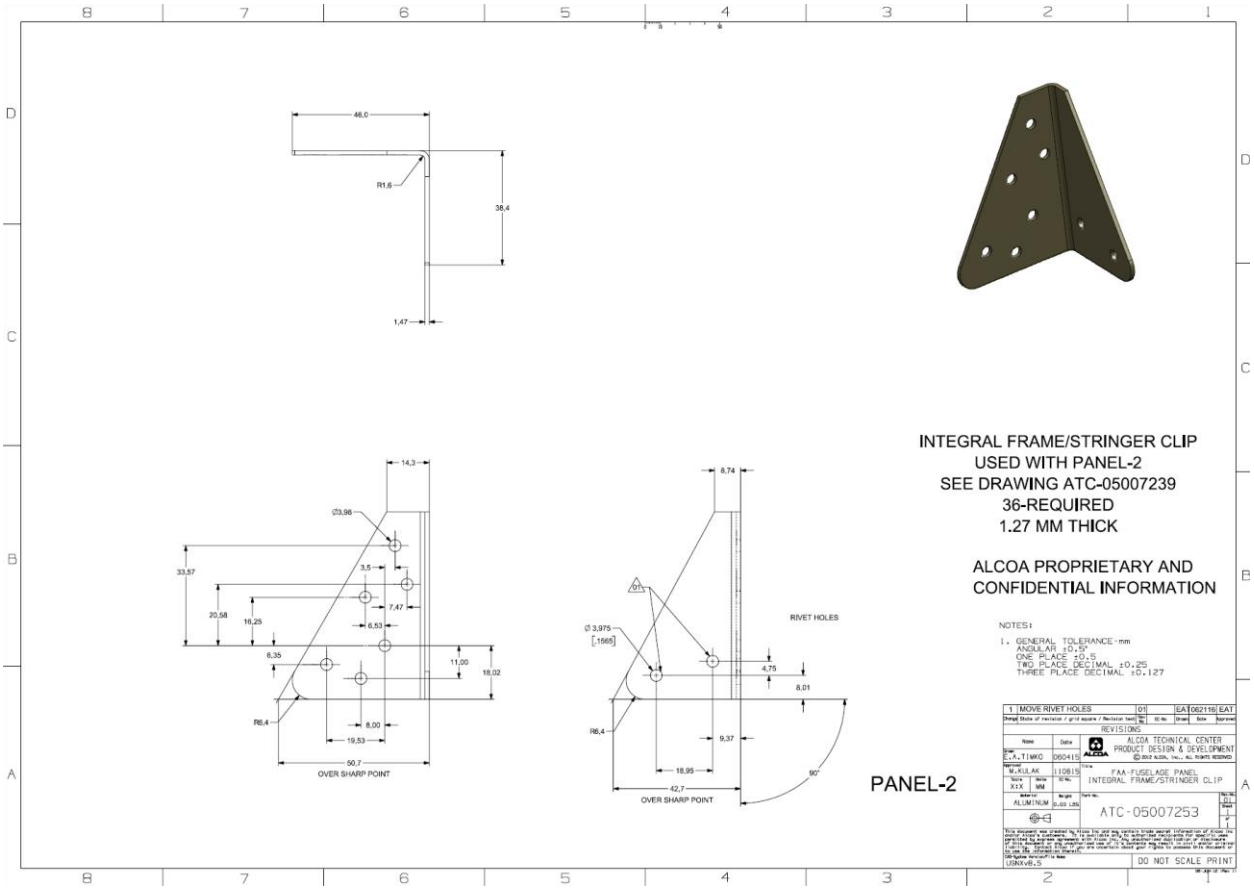

Figure A-10. Panel 2 stringer clip

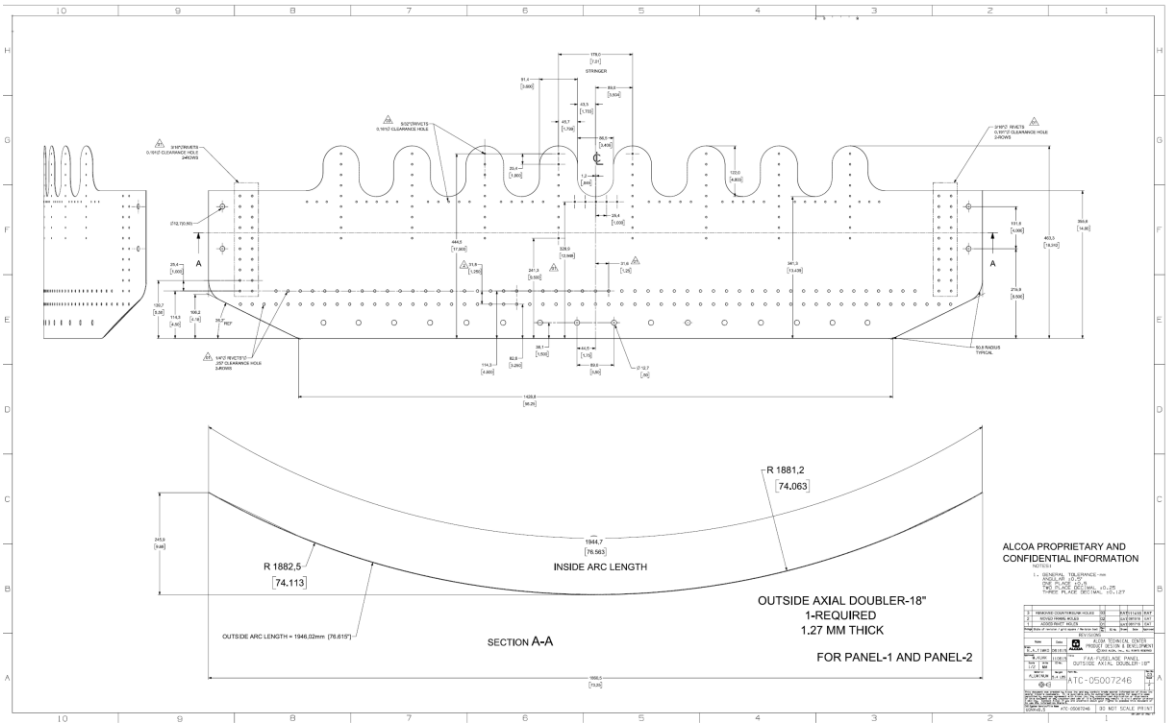

Figure A-11. Panel 2 axial edge doubler-1

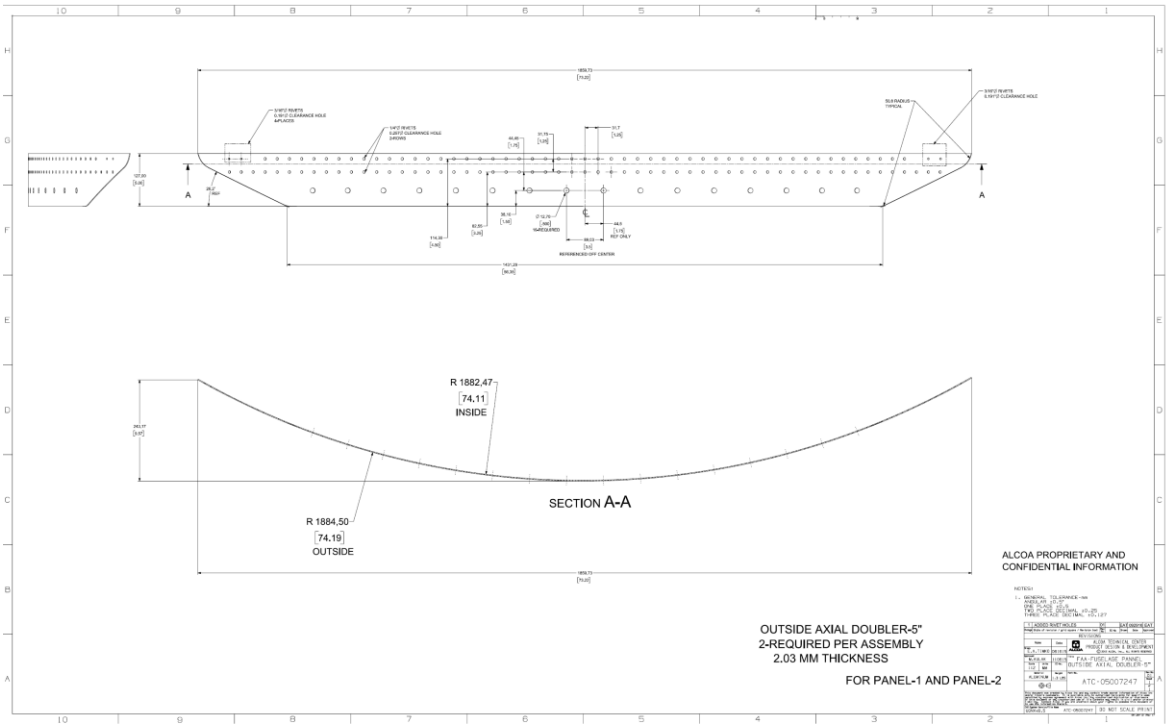

Figure A-12. Panel 2 outside axial doubler-5

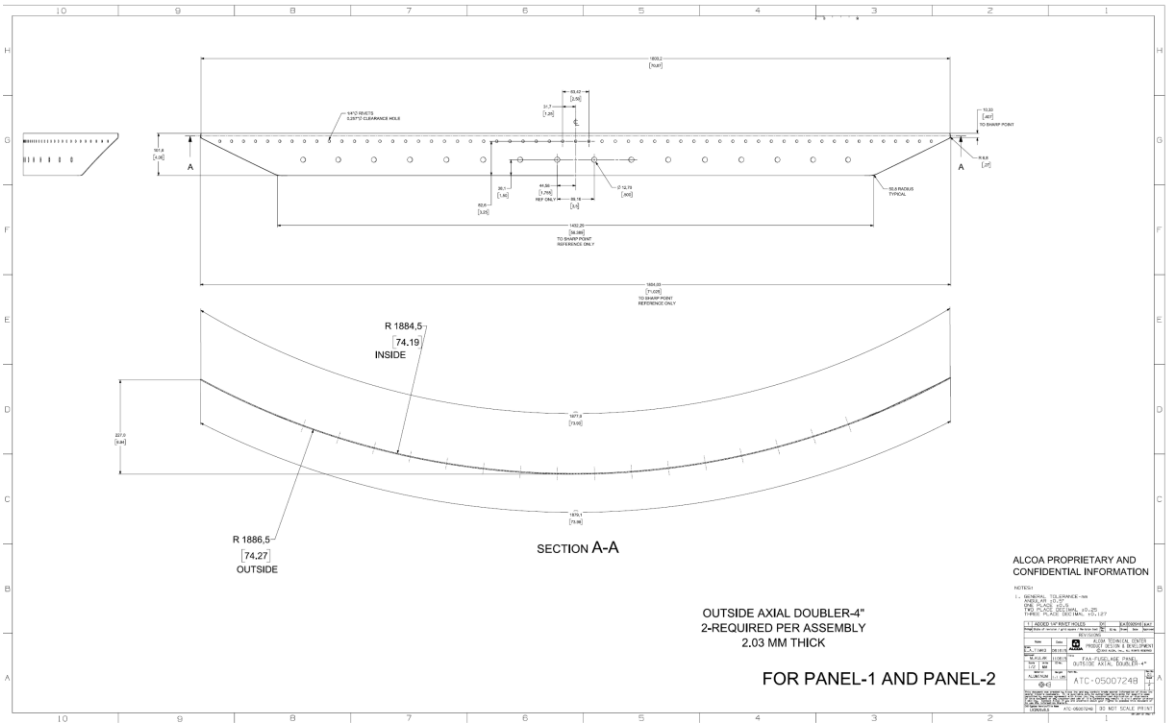

Figure A-13. Panel 2 outside axial doubler-4

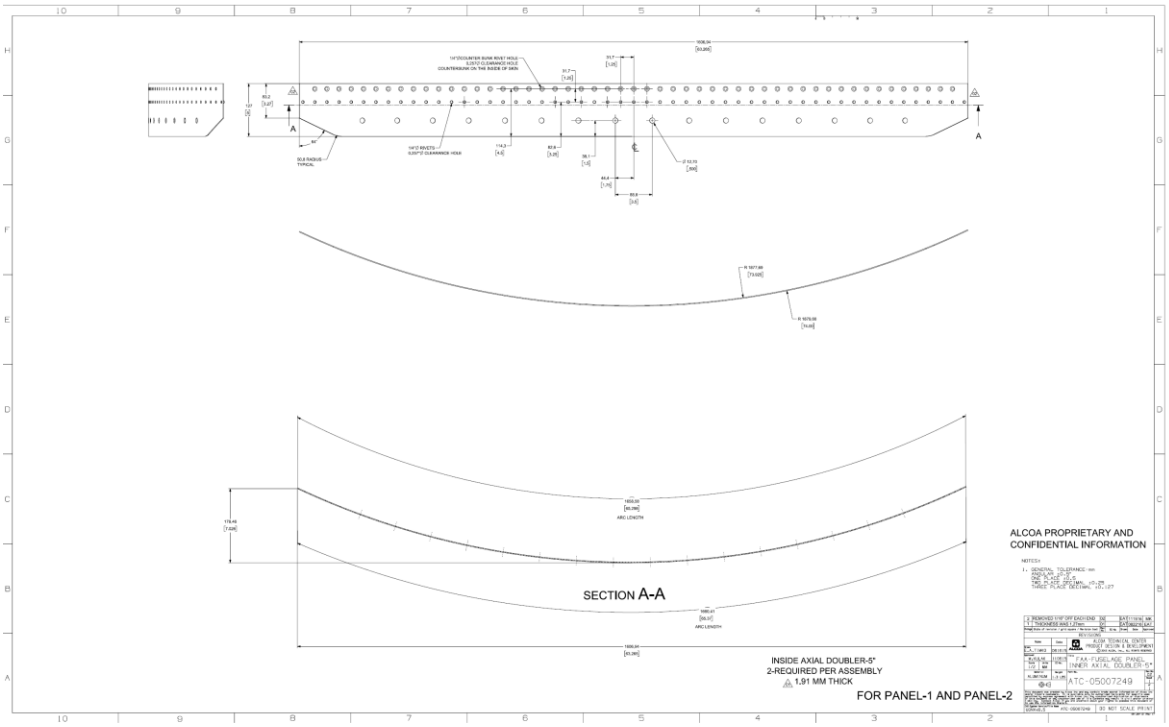

Figure A-14. Panel 2 inside axial doubler-5

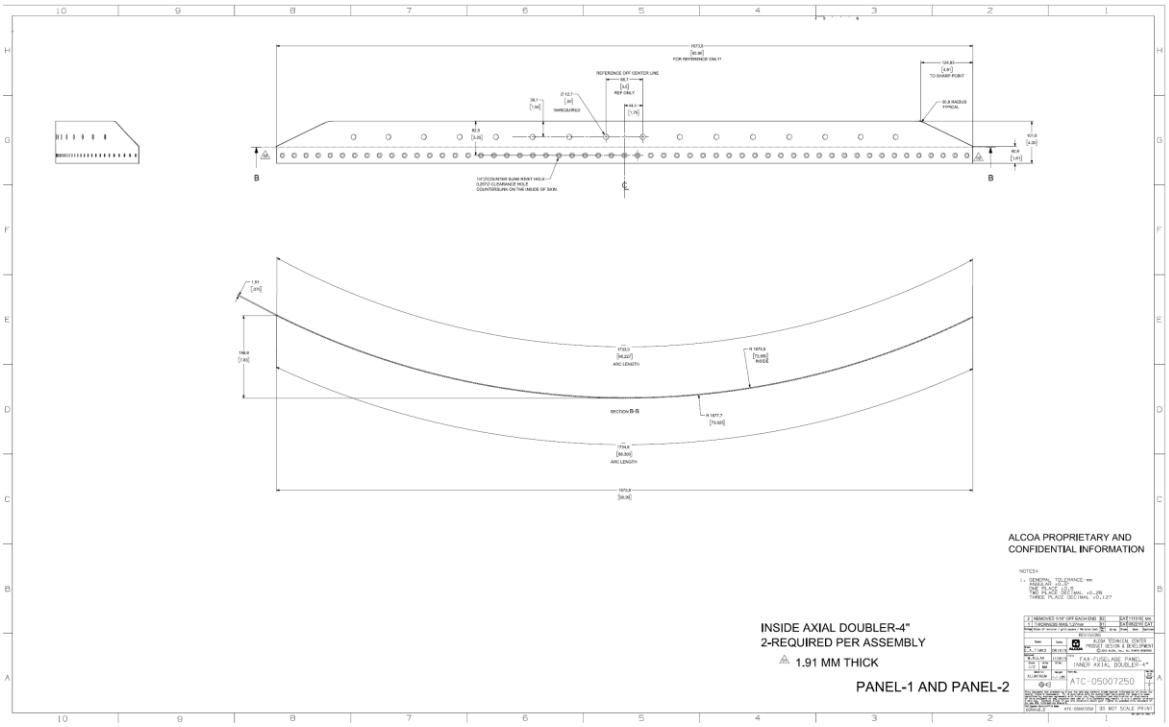

Figure A-15. Panel 2 inside axial doubler-4

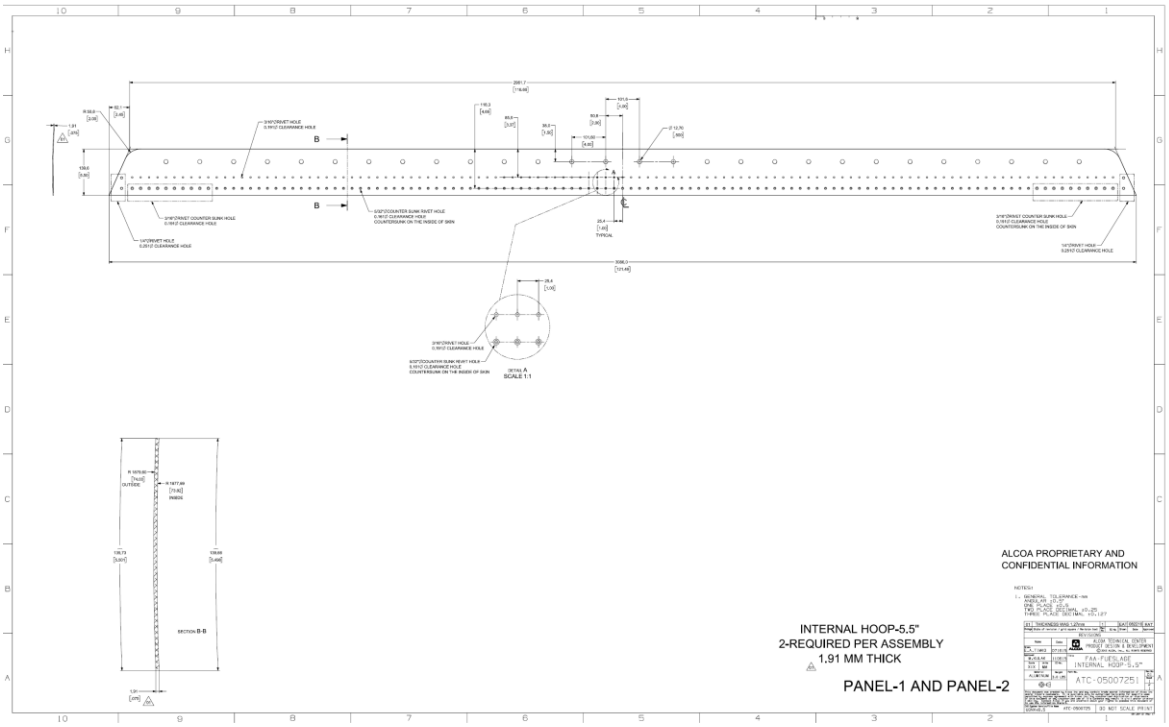

Figure A-16. Panel 2 inside hoop doubler-5

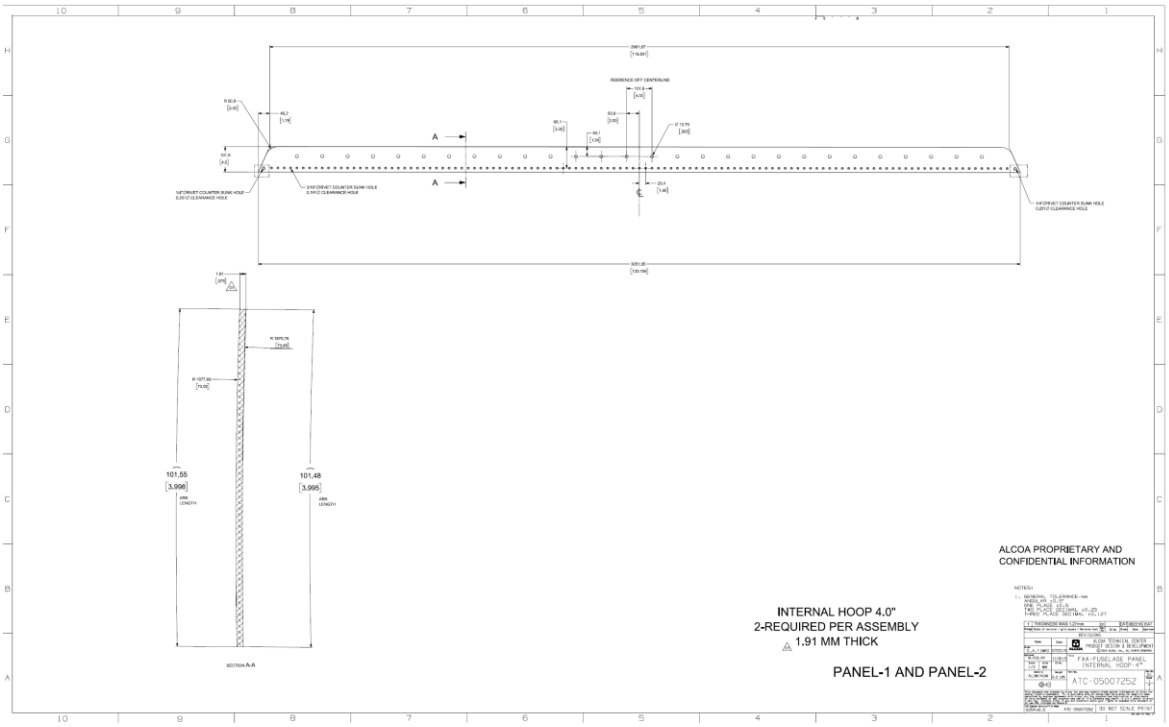

Figure A-17. Panel 2 inside hoop doubler-4

References

Kulak, M., Chang, P., Sklyut, H., & Heinimann, M. (2023). *Design, analysis and test development of full-scale fuselage test panels to assess emerging metallic structures technologies [DOT/FAA/TC-TNxx/x]*. Federal Aviation Adminstration.

Tian, Y., Stanley, D., & Backuckas, J. (2021). *Assessment of emerging metallic structures technologies through test and analysis of fuselage structure: Test panel 1 [DOT/FAA/TC-TN/21/25]*. Federal Aviation Administration.

B Phase 1 repair

At the end of Phase 1, the cracked structure needed to be repaired in order to continue with the testing phase. Phase 1 crack was repaired using Boeing 727 structural repair manual 53–30–3 as guideline. This appendix provides some details of the procedure and material used for the installation of SRM repairs.

Figure B-1shows the location of the SRM repair on Panel 2. Before the installation of the SRM repair, the surface of the skin was cleaned with acetone and dry air to remove any contaminants. Next, the eddy current system was used to mark the crack tips for both crack locations.

After marking the crack tips, further procedures were followed in accordance with the B727 SRM skin repair instructions. The basic requirement is that for a minimum of three rows of rivets beyond the damage cutout, the repair doubler should be one gage thicker than the skin material and it is acceptable to use button head rivets instead of countersunk rivets, as shown in Figure B-2. Figure B-3 shows the actual image of the SRM repairs after installation from both sides.

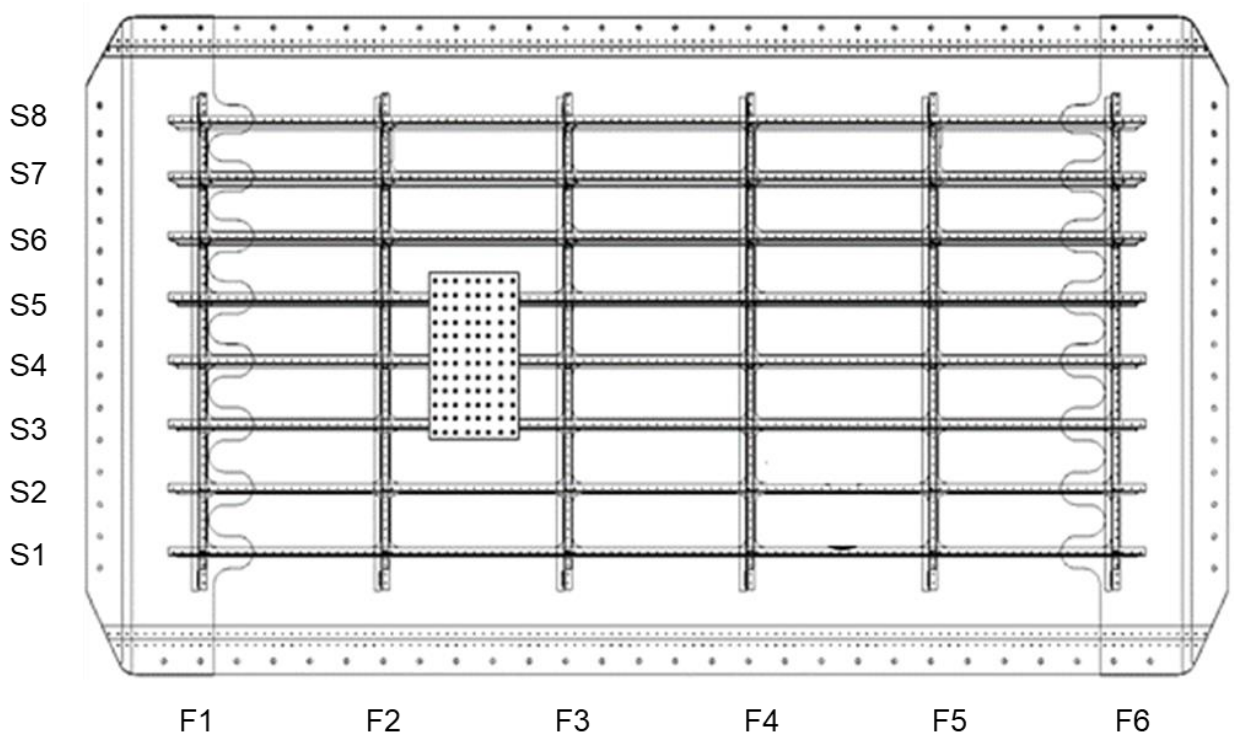

Figure B-1. Location of Phase 1 SRM repair

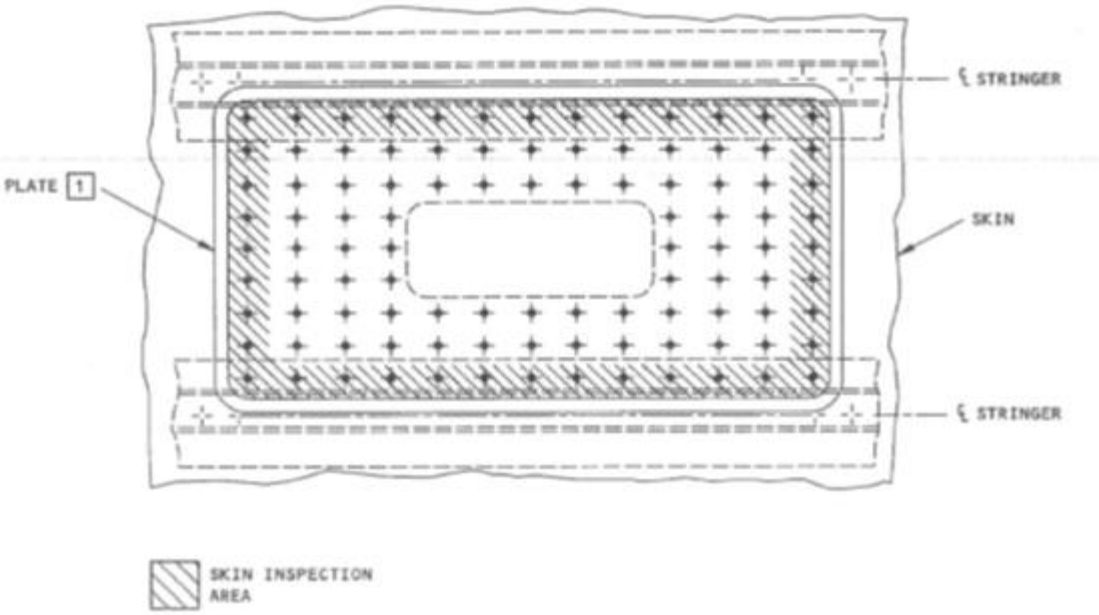

Figure B-2. Typical SRM skin repair configuration

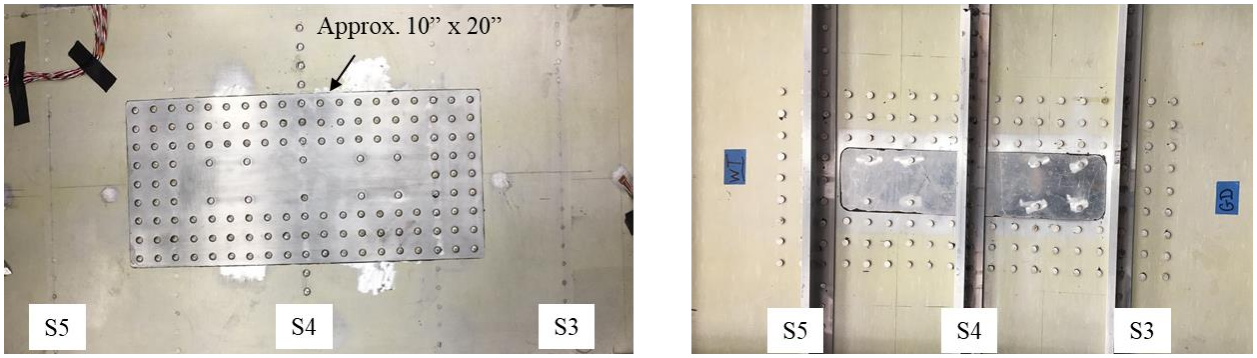

External view Internal view

Figure B-3. Phase 1 repair external and internal views

C Strain gage instrumentation

The test panel was fully instrumented with strain gages within the test section to provide for real-time monitoring of the panel strain distributions. A total of 144 strain gage channels were used, including 34 rosette gages, 20 uniaxial gages on stringers, 18 uniaxial gages on frame flanges, and two uniaxial gages on a phase three stringer clip, as shown from Figure C-1 to Figure C-4. The locations of strain gages installed on the skin, frames, and stringers for each test phase are provided from Figure C-5 to Figure C-10.

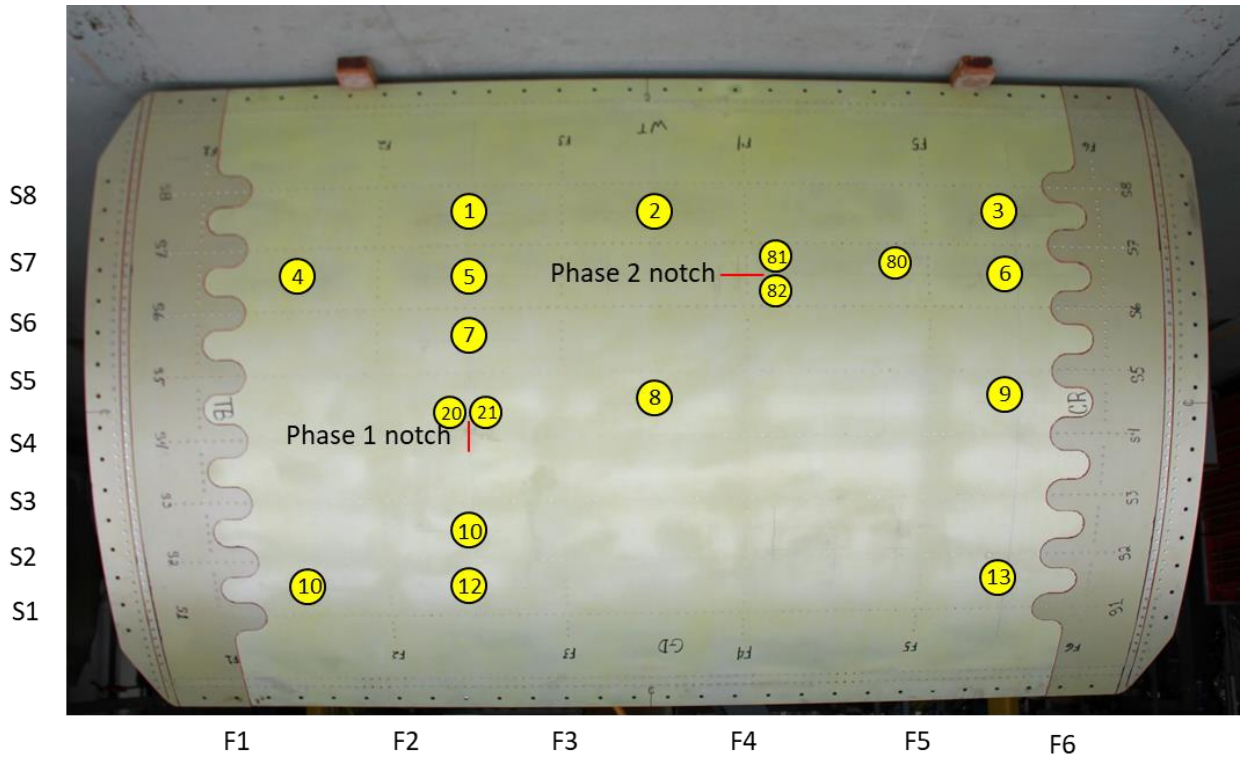

Figure C-1. Picture of external rosette gages

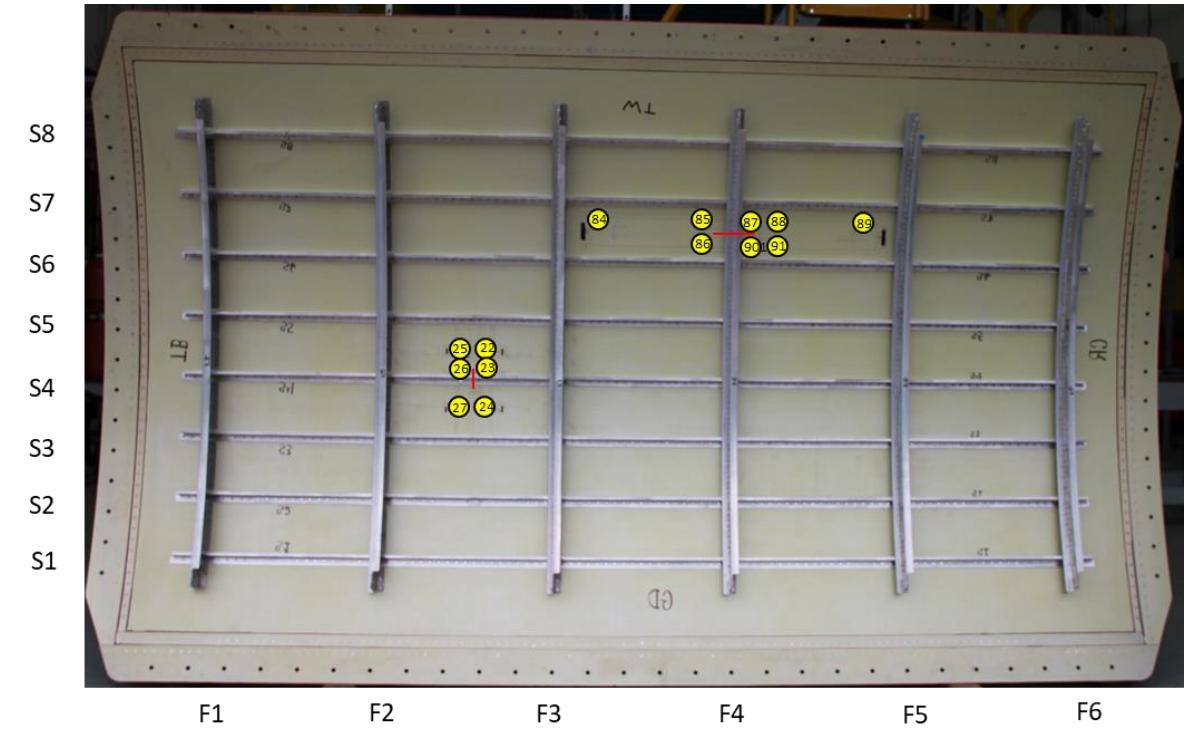

Figure C-2. Picture of internal rosette gages

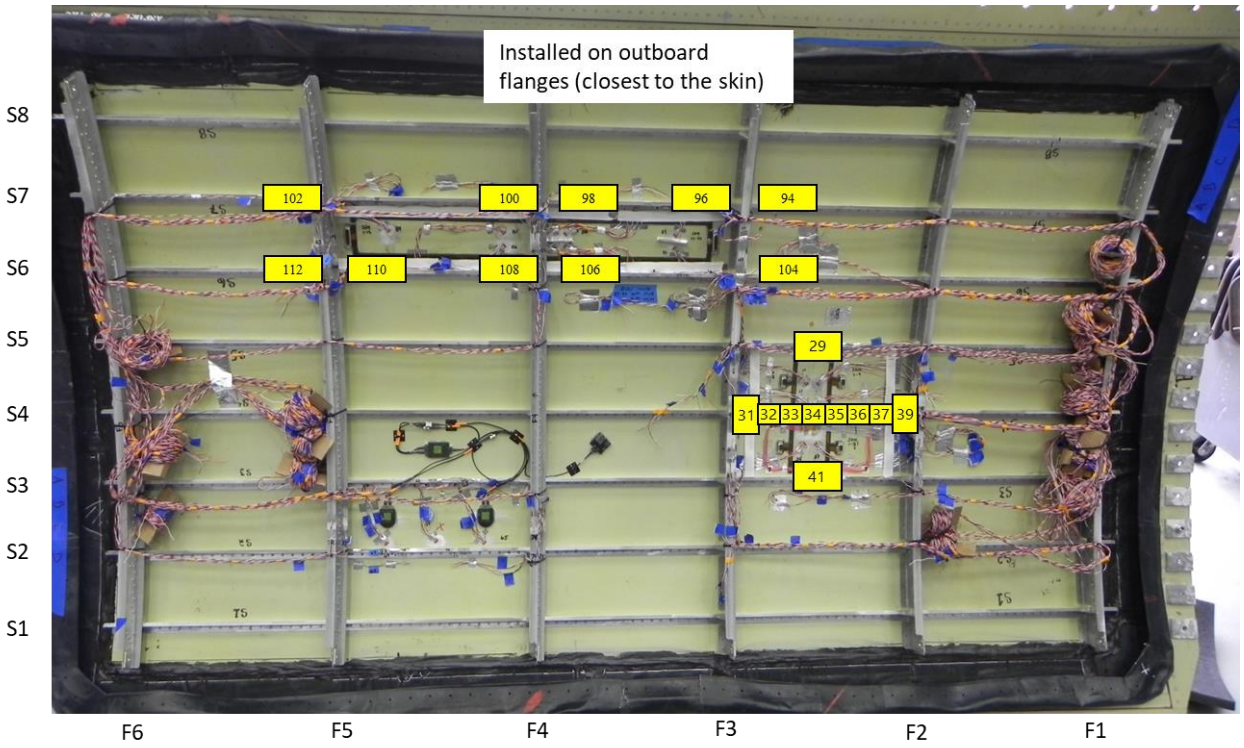

Figure C-3. Picture of stringer gages

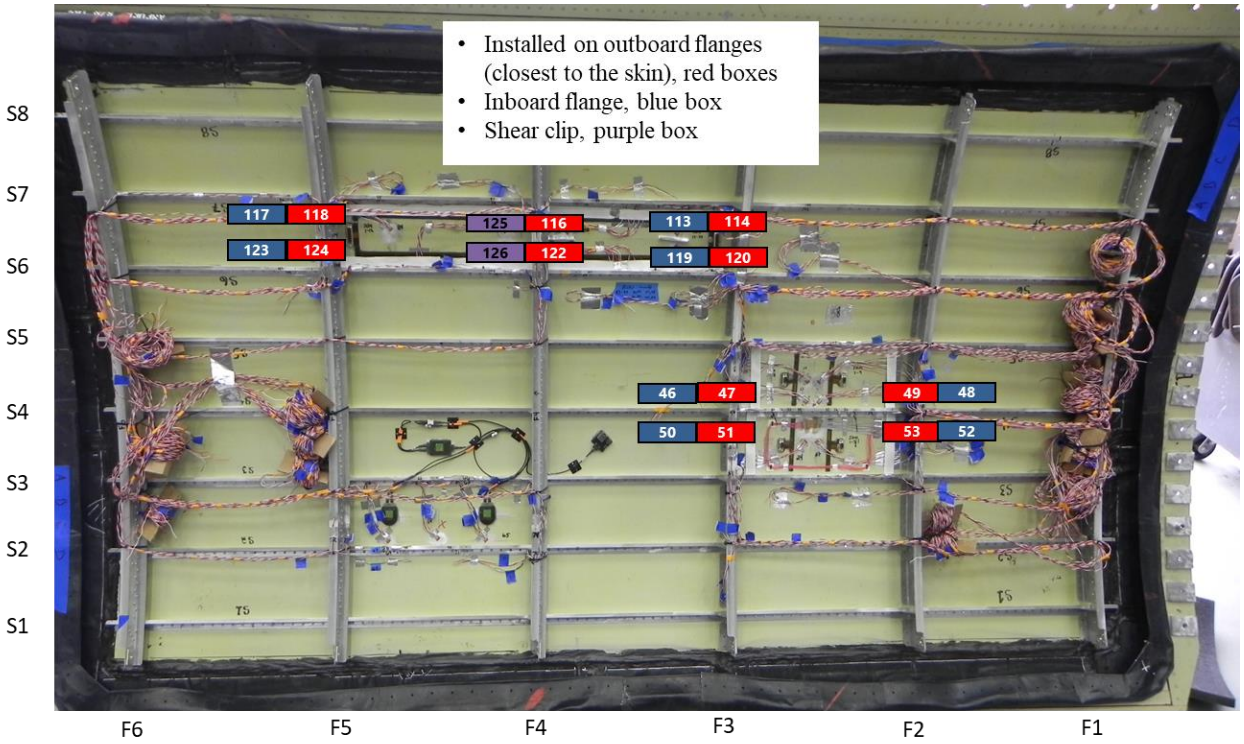

Figure C-4. Picture of frame gages and stringer clip gages

Strain readings were recorded during holds occurring at equal load intervals up to the maximum applied loads during strain surveys. In addition, data was continuously recorded at a frequency of 1 Hz and at each endpoint to monitor the strains during the test. Strain gages at mid-bay locations that were monitored throughout all phases are shown in Figure C-5.

The test panel was instrumented with strain gages to meet the following considerations:

1. Strain gages were strategically placed on the test panel to compare with the FEM analysis results. The gages were placed on the skins, stringers, and frames for the circumferential crack and longitudinal crack, to confirm the variation in stress in these critical areas before cracks are inserted.

2. The gages were placed strategically close to the crack tip to confirm stresses once cracks start growing.

3. Strain gages were also placed at other strategic locations of the panel to compare with the FEM results based on prior experience the FAA has gained from testing panels.

The wires for strain gages that pass through the inside of the pressure box were Teflon-coated to prevent water damage. A lead wire minimum length of 15 feet extending outside the pressure box was soldered to each strain gage channel. Readouts for all strain gages were monitored periodically and permanently recorded during the fatigue test and during strain survey under mechanical loading.

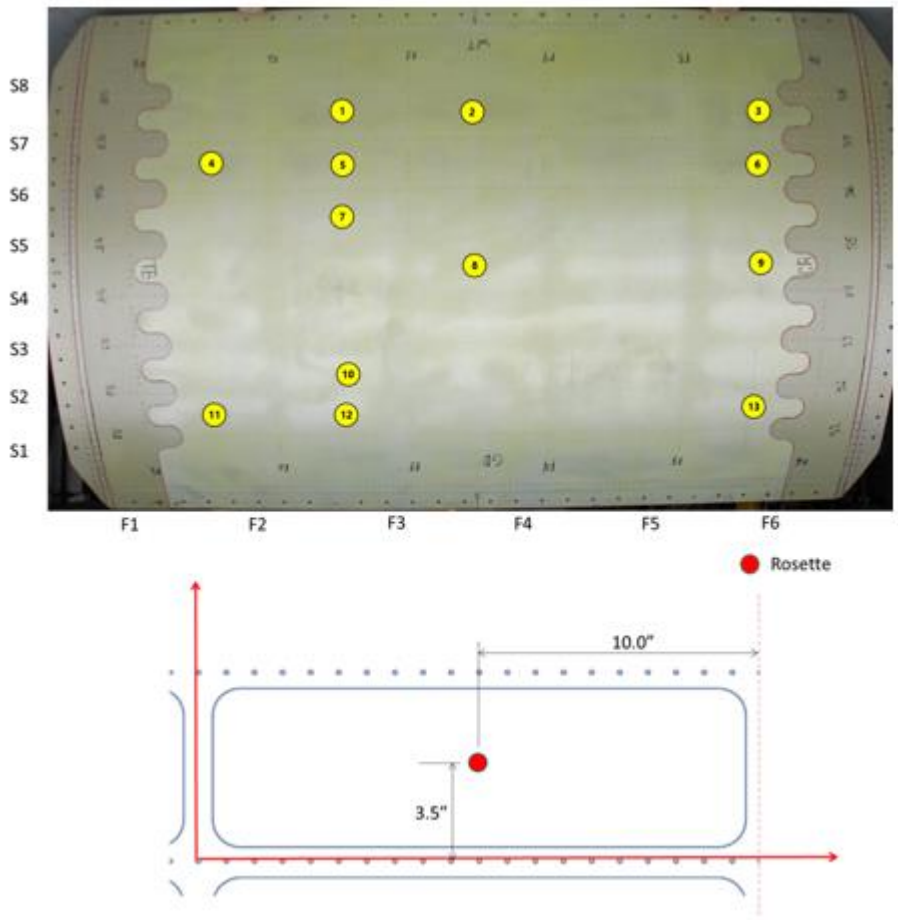

Figure C-5. Mid-bay location strain gages

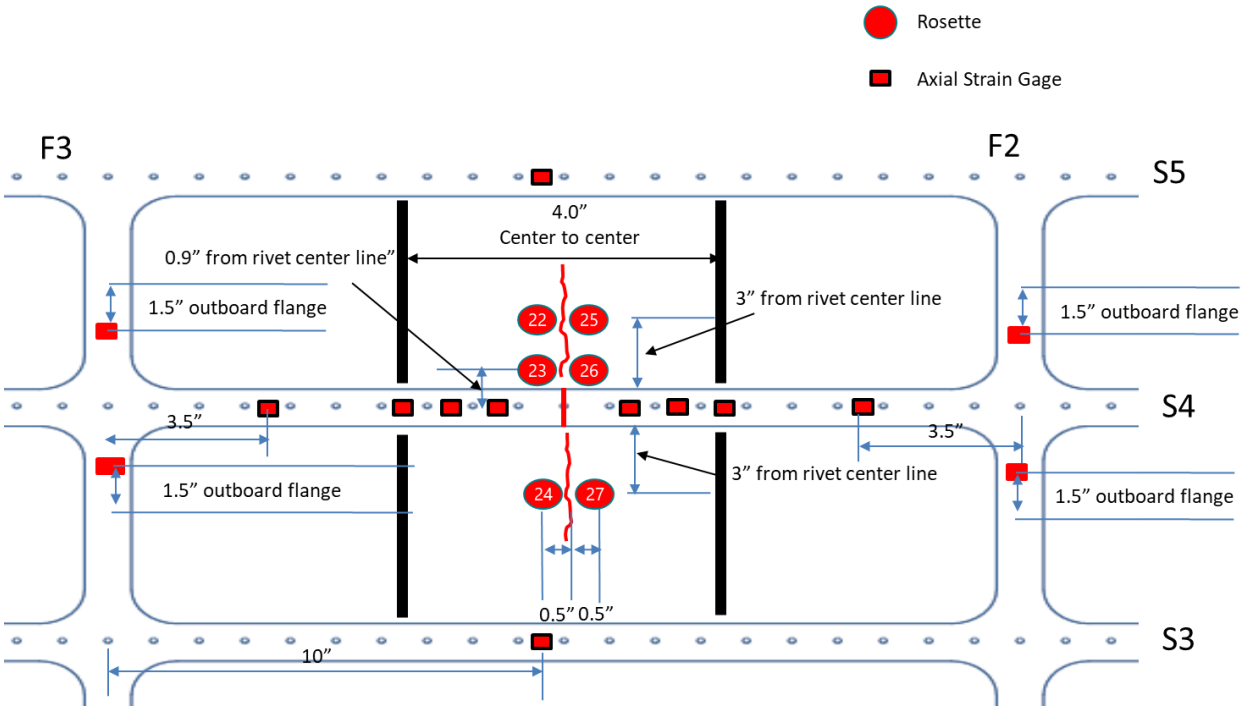

Figure C-6. Phase 1 internal gages

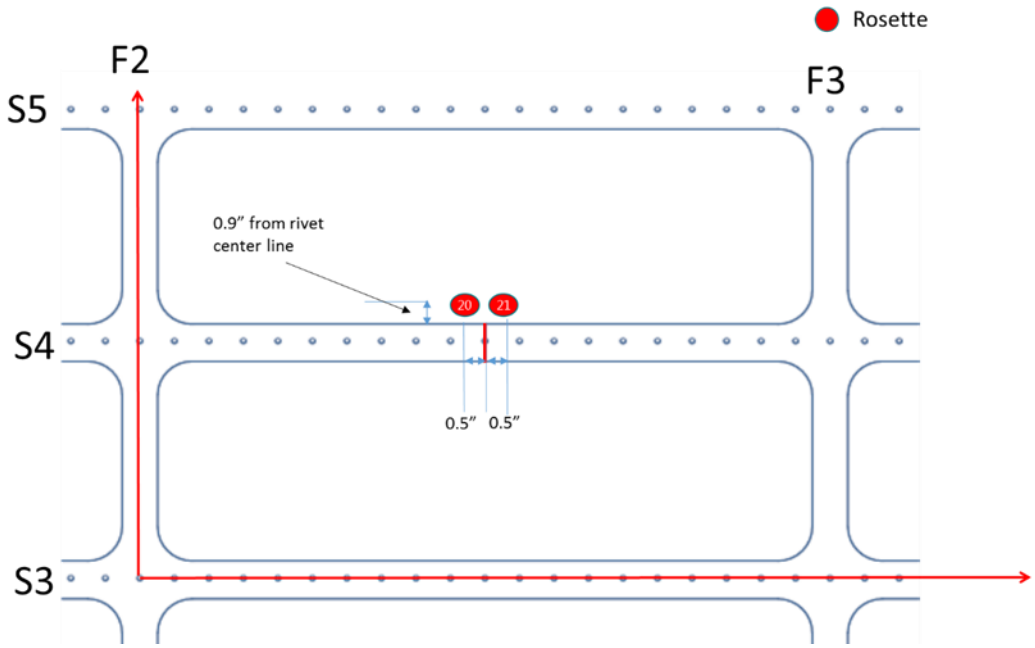

Figure C-7. Phase 1 external skin gages

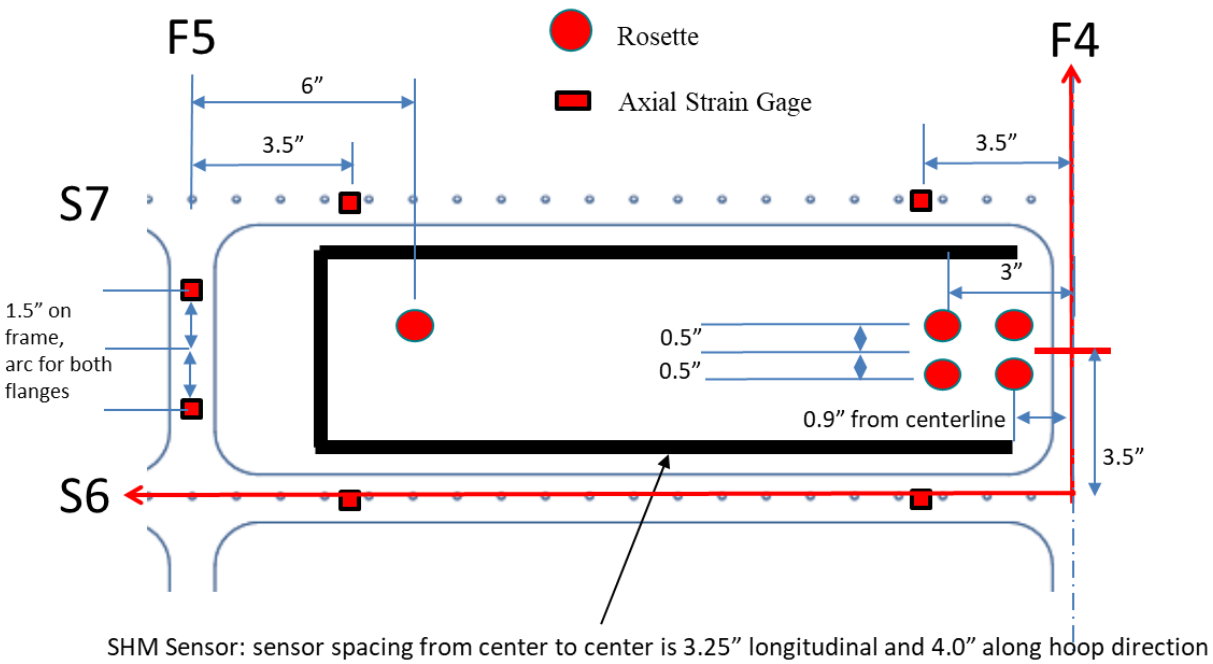

Figure C-8. Phase 2 internal gage: left side

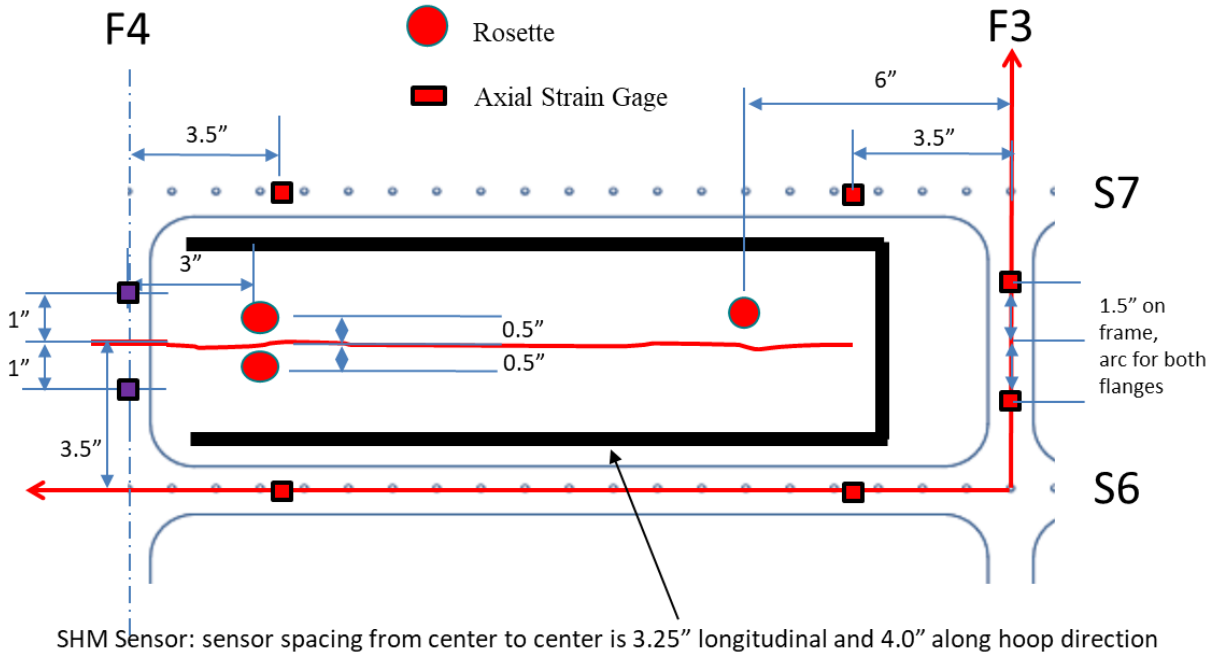

Figure C-9. Phase 2 internal gages: right side

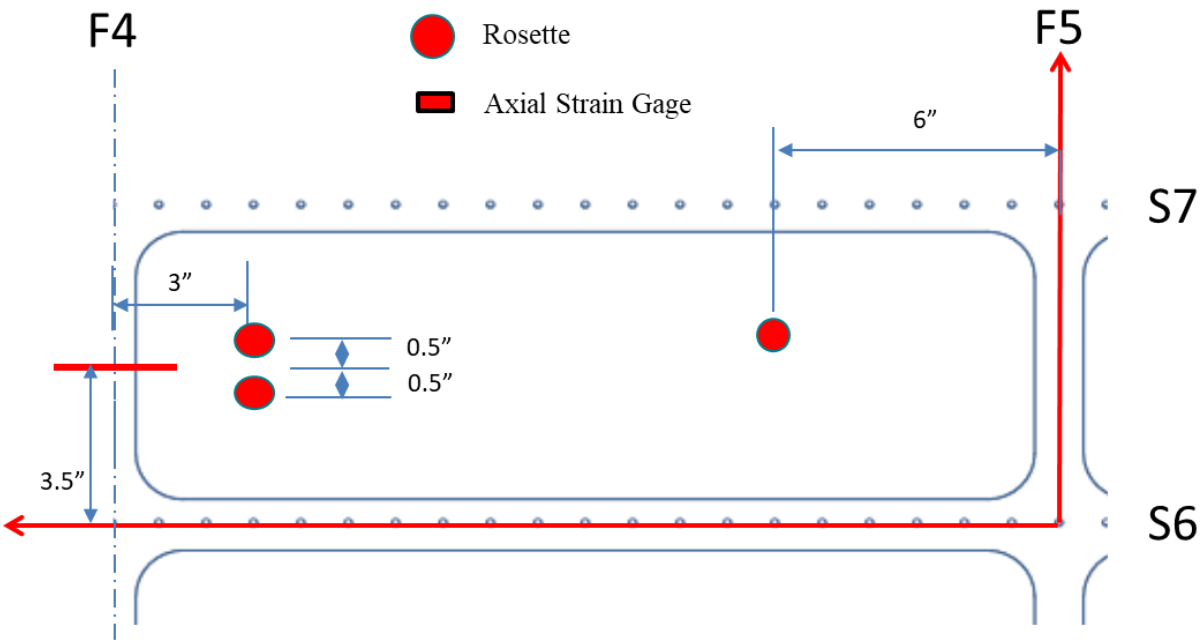

Figure C-10. Phase 2 external gages

D ARAMIS digital image correlation system

Full-field deformation and strain data were recorded during the loading of the test panels using the ARAMIS™ three-dimensional digital image correlation (DIC) system. The system, which uses two 5-megapixel cameras, is capable of accurately measuring full-field strain within 50 με. The typical system setup and stochastic pattern used are shown in Figure D-1.

Prior to testing, the areas to be monitored by the photogrammetry system were coated with a high-contrast, stochastic speckle pattern. Flat-black spray paint was used to create a random pattern on top of a flat white layer. The coarseness of the pattern directly affects the resolution of the measured strain field. Baseline images were taken using both cameras at zero loads. Deformed images were recorded using both cameras while under an applied load. The baseline and deformed images are then used to determine the full-field deformation and strain field.

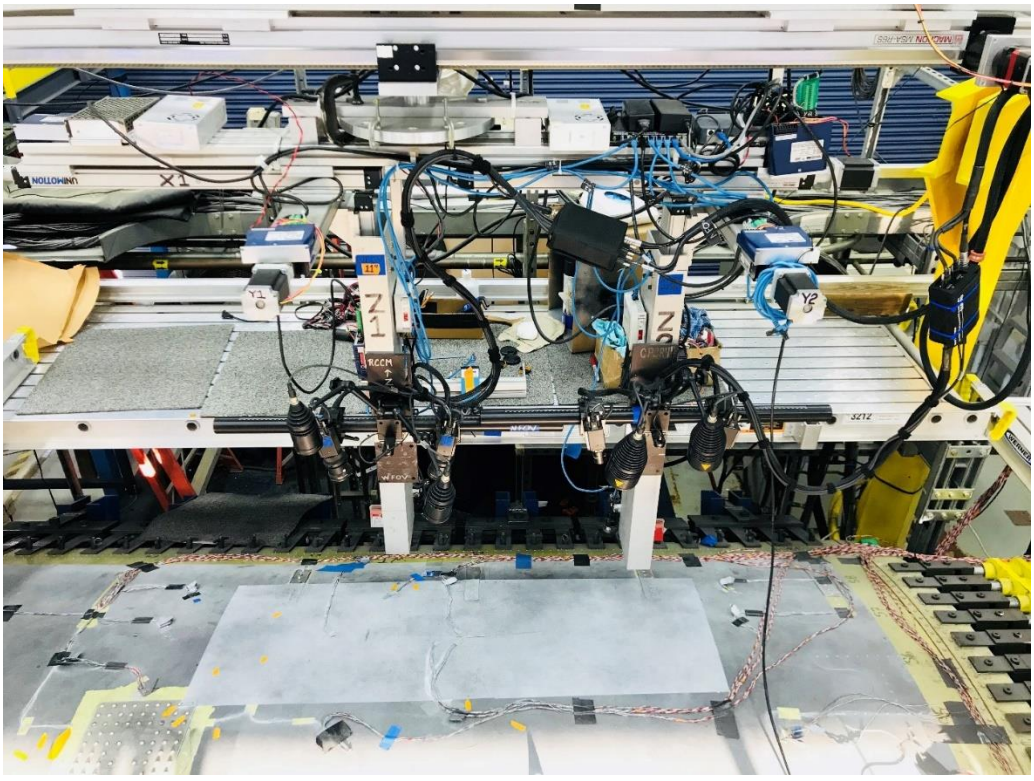

Figure D-1. ARAMIS system setup and stochastic pattern on panel

E Structural health monitoring system

Structural Health Monitoring (SHM) systems will be used to monitor and record damage growth: an Acellent system for Phase 1 circumferential cracks and Phase 2 longitudinal cracks, and a Metis design system for Phase 1 circumferential cracks, as shown in Figure E-1 and Figure E-2. Both systems consist of three major components: piezoelectric sensors, hardware, and software. Both systems use piezoelectric sensors to create an ultrasonic wave to interrogate the part. Installation of sensors is similar to bonding a strain gage in terms of surface preparation and time required. Sensor locations and cables were routed to prevent interference with strain gages and connected to a data acquisition unit. Data was recorded during periodic inspection of the test article.

Acellent and Metis Design trained Federal Aviation Administration (FAA) personnel on how to install sensor and collect the data during panel 1 test. The sensors were installed by FAA personnel on panel 2. The testing was stopped periodically for inspection, in accordance with the test procedures, SHM data was collected during the inspections. The details of sensor description and installation procedure were provided in (Tian, Y., 2021).

The Tech Center used algorithms developed by Embraer, Boeing, and Sikorsky to assist in the analysis of the SHM systems, and the results will be published in a separate technical note.

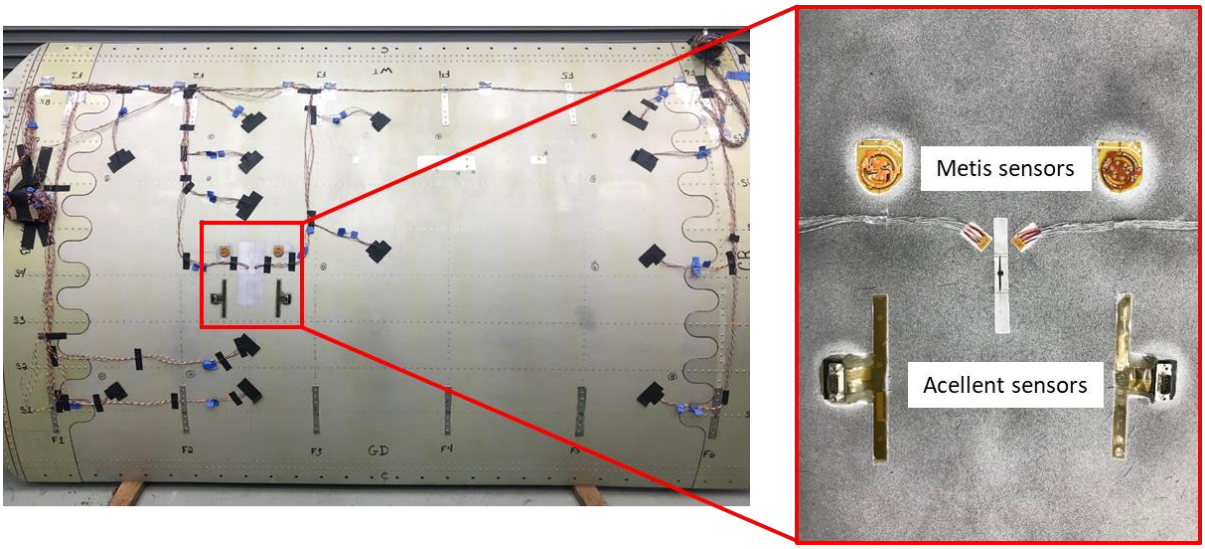

Figure E-1. SHM sensor locations for panel 2 phase 1

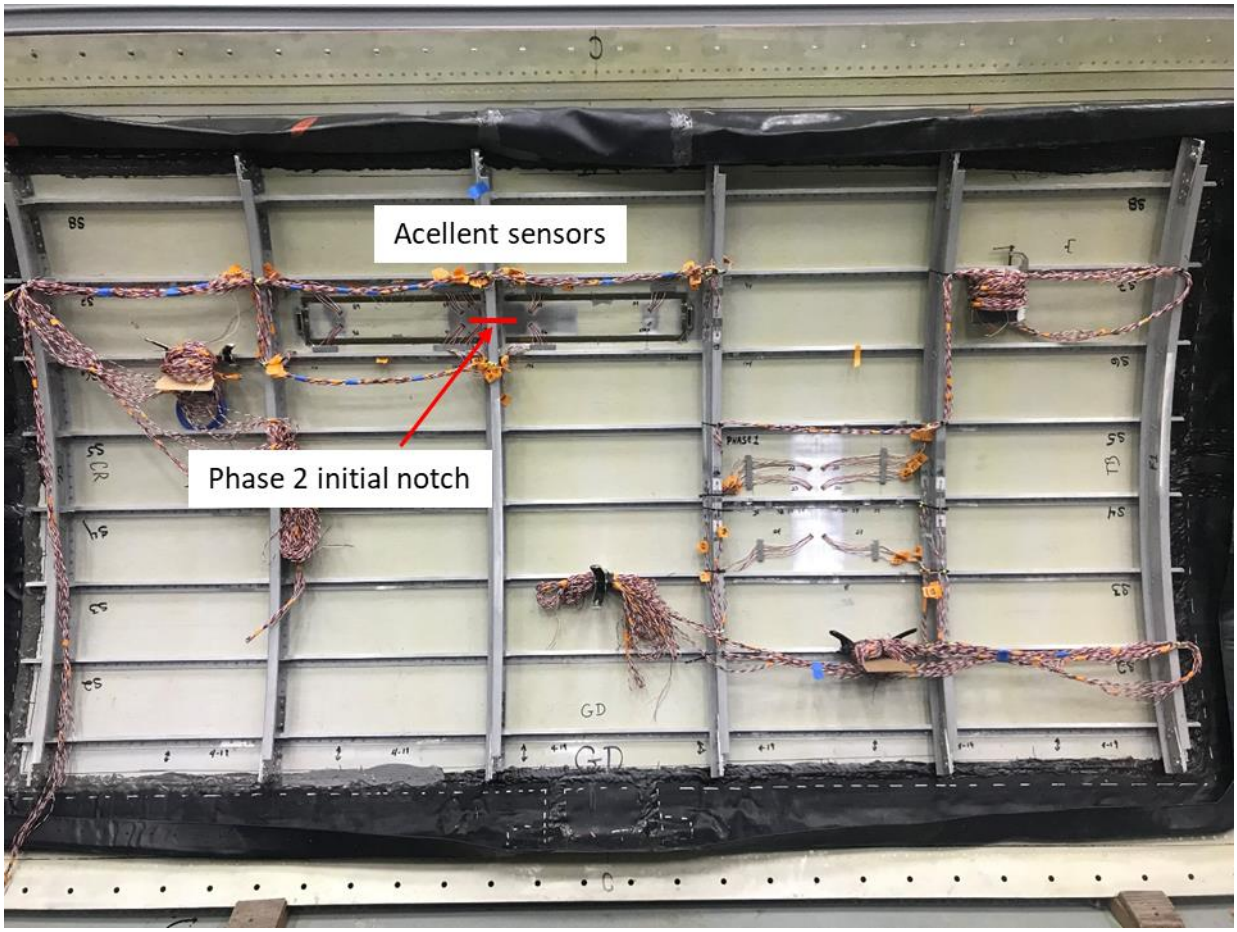

Figure E-2. SHM sensor locations for panel 2 phase 2

References

Tian, Y., Stanley, D., & Backuckas, J. (2021). *Assessment of emerging metallic structures technologies through test and analysis of fuselage structure: Test panel 1 [DOT/FAA/TC-TN/21/25]*. Federal Aviation Administration.

F Frame reinforcement repair

One lesson learned from panel 1 testing is that the frame ends need to be reinforced to avoid crack induced premature failure. Therefore, all frame ends were reinforced using doubler on both sides before the installation of panel on the fixture as shown in Figure F-1 . The design and installation of the frame reinforcement were found structurally sufficient to sustain both fatigue, limit load test, and residual strength test.

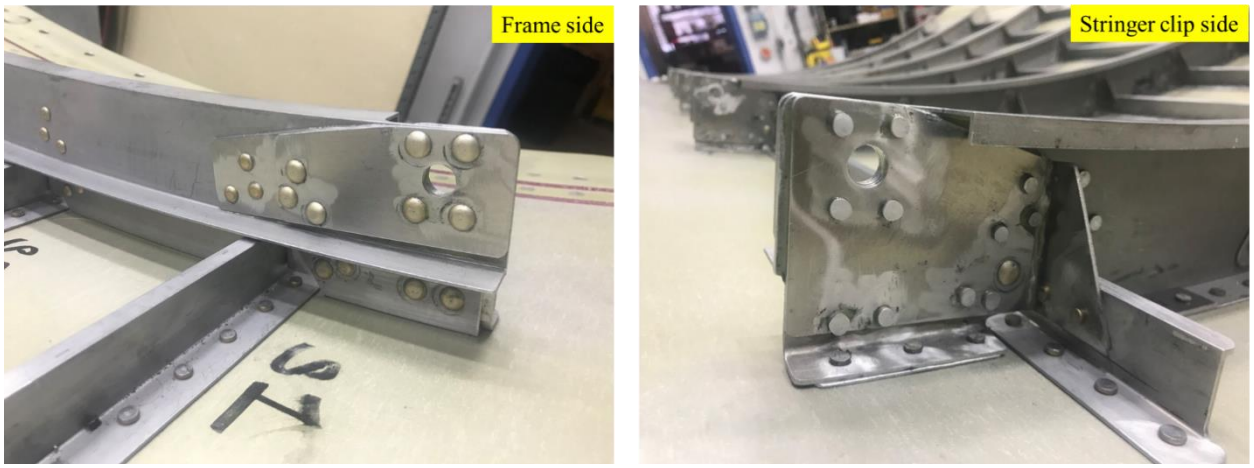

Figure F-1. Configuration of frame reinforcement repair from both ends